

Experimental and Theoretical Studies on the Mechanism of the C–S Bond Activation of Pd^{II} Thiolate/Thioether Complexes

Sushil Kumar,[†] Fabrice Guyon,^{*,†} Michael Knorr,[†] Stéphane Labat,[‡] Karinne Miqueu,^{*,‡} Christopher Golz,[§] and Carsten Strohmann[§]

[†]Institut UTINAM, UMR CNRS 6213, Université Bourgogne Franche-Comté, Faculté des Sciences et des Techniques, 16 Route de Gray, 25030 Besançon, France

[‡]CNRS/UNIV PAU & PAYS ADOUR, Institut des Sciences Analytiques et de Physico-Chimie pour l'environnement et les Matériaux, UMR 5254, 64000 Pau, France

[§]Technische Universität Dortmund, Anorganische Chemie, Otto-Hahn Strasse 6, 44227 Dortmund, Germany

Supporting Information

ABSTRACT: Two equivalents of **L** (**L** = 4-methylthio-2-thioxo-1,3-dithiole-5-thiolate or Medmit) react with *cis*-Pd-(PR₃)₂Cl₂ (R = Ph and Et) to afford Pd(PR₃)₂(η¹-L)(η²-L) (R = Et: **1**; R = Ph: **2**) complexes, which have been characterized by X-ray crystallography. These compounds are dynamic in solution due to an exchange of the thiomethyl groups on palladium. Variable-temperature ¹H NMR spectroscopy reveals a low coalescence temperature (173 K). Treatment of Pd(*diphos*)Cl₂ (*diphos* = dppe or dppm) with 2 equiv of **L** affords thiolato complexes Pd(dppe)(η¹-L)₂ (**3**) and Pd(dppm)(η¹-L)₂ (**4**). Whereas **3** is rigid in solution with firm η²-coordination of dppe and η¹-coordination of the thiolate, two linkage isomers Pd(η²-dppm)(η¹-L)₂ and Pd(η¹-dppm)(η¹-L)(η²-L) coexist in a solution of **4**. **L** coordinated on Pd^{II} undergoes a S-demethylation reaction leading to dithiolene complexes and MeL. This transformation requires high temperature, and its efficiency depends on the nature of the phosphines as well as the nature of the metal (Pd vs Pt). DFT calculations reveal that the most likely mechanism depends on the lability of phosphines. Starting from M(PR₃)₂(η¹-L)₂ (M = Pd and Pt; R = Ph and Et), the favored sequence implies decooordination of one triethyl phosphine (M(PEt₃)(η¹-L)(η²-L)₂ as intermediate) or two triphenylphosphines (Pd(η²-L)₂ as intermediate) followed by oxidative addition and reductive elimination (OA/RE) reactions. In the case of PEt₃, this OA/RE sequence can also compete with an intramolecular nucleophilic addition (A_N), which can be described as an attack of a thiolate sulfur atom on a CH₃⁺ carbocation. An intramolecular S_N2 process was found to be the most feasible, starting from M(dppe)(η¹-L)₂ (M = Pd and Pt), with the nucleophile approaching the thiomethyl group at an angle of 180° with respect to the C_{CH₃}–S bond. The influence of the coligand has also been studied experimentally. Structurally characterized disulfide L–L dimer has been isolated upon reaction of 2 equiv of **L** with MCl₂ (M = Pd and Pt).

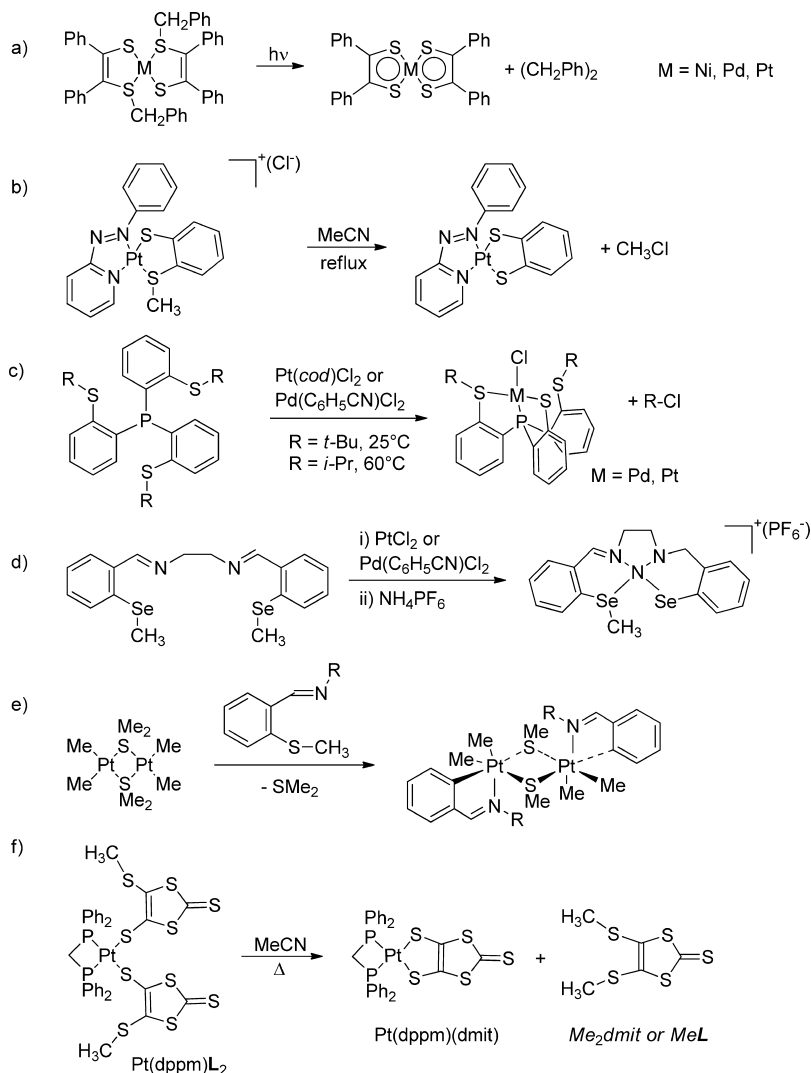


INTRODUCTION

Since the first report on a C–S bond activation, namely, the S-dealkylation of dimethylsulfide by PtCl₂ dating from 1883,¹ this topic is still of interest. Driven primarily by interests in the hydrodesulfurization of fossil fuels, various aspects of the C–S activation process have been since extensively studied allowing the development of new synthetic methods including stoichiometric as well as catalytic reactions.² An interesting class of compounds which undergo S-dealkylation reactions are the group 10 EηS_{thioether} chelate complexes (E = Ni, Pd, Pt, and Pt).³ In the latter, the C–S_{thioether} cleavage may be homolytic and photochemically induced as in Ni⁰ complexes of 2-(diphenylphosphino)thioanisole⁴ and in bis(S-benzyl-1,2-diphenyl-1,2-ethylenedithiolato)M^{II} (Ni, Pd, and Pt) complexes (Scheme 1a).⁵ Dealkylation reactions occur also heterolytically by reaction with nucleophiles such as amines or chloride. Such an alkyl transfers to nucleophiles have been characterized as Menschutkin-type S_N2 reactions.⁶ This substitution is favored

by complexation of the thioether group to the metal center, imparting a diminution of electron density at the sulfur atom and consequently an increase of electrophilicity of the C atom bonded to this sulfur. Moreover, this transformation is driven thermodynamically by the conversion of a dative S_{thioether} → M interaction in a strong covalent M–S_{thiolate} bond. The nature of ancillary ligand also impacts the S–C bond cleavage. Goswami et al. have studied the reaction of 2-methylthioaniline with Pt(*pap*)Cl₂ (*pap* = 2-(phenylazo)pyridine) and Pt(*bpy*)Cl₂ (*bpy* = 2,2'-bipyridine).⁷ A rupture of the H₃C–S bond was observed with the strong π-acidic coligand *pap* to afford Pt(*pap*) (HNηS) (Scheme 1b), whereas the 2,2'-bipyridine ancillary ligand failed to promote the demethylation of Pt(*bpy*) (HNηSCH₃). Recently, the activation of the C–S bond of the PS₃-type tripodal tetradentate ligands, tris(2-*tert*-

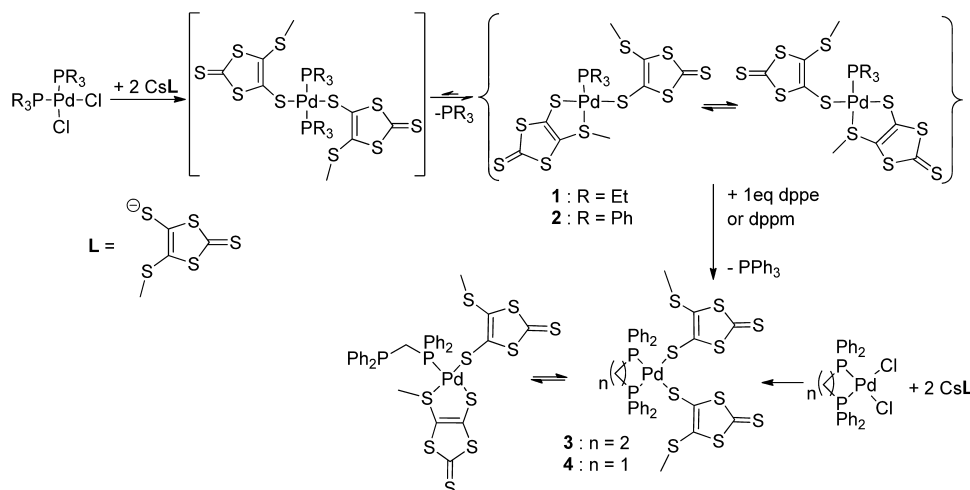
Received: January 16, 2017

Scheme 1. Examples of C–S Bond Activation of E \cap S_{thioether} Ligands (E = N, P, S, and Se)

butylthiophenyl)phosphine and tris(2-isopropylthiophenylphosphine), by group VIII metal compounds has been studied in depth.⁸ Reaction of tris(2-*tert*-butylthiophenyl)phosphine with $\text{PdCl}_2(\text{PhCN})_2$ and $\text{PtCl}_2(\text{cod})$ at room temperature resulted in the elimination of *t*-BuCl and formation of $\text{MCl}\{\text{P}(2\text{-SC}_6\text{H}_4)(2\text{-}t\text{-BuSC}_6\text{H}_4)_2\}$ (Scheme 1c). In contrast, the C–S activation in the isopropyl derivatives required more forcing conditions (333 K). The more facile elimination of *t*-BuCl compared to that of *i*-PrCl was attributed to the higher stability of the *tert*-butyl cation vs an isopropyl cation. In the case of bis(methyl)selenosalen and bis(methyl)thiasalen podands (Scheme 1d), the mechanistic pathway of the $\text{S}_{\text{N}}2$ substitution at the methyl group by chloride (stemming from the inorganic starting metallic salts) has been theoretically compared to that of a process implying an oxidative addition of the chalcogen– C_{alkyl} bond on Pd^{II} or Pt^{II} followed by reductive elimination of alkyl chloride. DFT calculations indicated that the experimentally observed chalcogen– C_{alkyl} bond activation occurred more likely via $\text{S}_{\text{N}}2$ mechanism instead of a sequence implying changes in oxidation state of the metal.⁹ However, the oxidative addition of a C–S bond on a Pt^{II} has been recently observed in a $\text{PtMe}_2(\text{RN}\cap\text{SCH}_3)$ ($\text{RN}\cap\text{SCH}_3 = 1,2\text{-C}_6\text{H}_4(\text{CH}=\text{NR})(\text{SCH}_3)$), and the resulting dinuclear Pt^{IV} thiolate complex has been characterized (Scheme 1e). Note

that in this case the activation involves an aryl–sulfur bond instead of an alkyl–sulfur bond.¹⁰ We reported previously that thiolates $\text{trans-Pt}^{\text{II}}(\text{PEt}_3)_2(\eta^1\text{-L})_2$ and $\text{Pt}^{\text{II}}(\text{dppm})(\eta^1\text{-L})_2$ ($\text{L} = 4\text{-methylthio-2-thioxo-1,3-dithiole-5-thiolate}$ or *Medmit*; *dppm* = 1,1-bis(diphenylphosphanyl)methane) undergo S-demethylation by heating in acetonitrile or toluene solutions, yielding dithiolene complexes $\text{Pt}^{\text{II}}(\text{PEt}_3)_2(\text{dmit})$ and $\text{Pt}^{\text{II}}(\text{dppm})(\text{dmit})$ along with *MeL* (Scheme 1f).¹¹ A sequence implying S–CH₃ oxidative addition followed by reductive elimination driven by the formation of a stable dithiolene chelate complex was proposed, although no Pt^{IV} intermediate could be evidenced. The intramolecular C–S oxidative addition on a low-valent transition metal requires the proximity of the thioether fragment to the latter.¹² With hemilabile L ligand (η^1 -thiolate or η^2 -thiolate/thioether coordination mode), the nature of the metal and that of the coligands may affect the $\text{CH}_3\text{S} \rightarrow \text{M}$ dative interaction and consequently the reactivity of coordinated L. Our experimental investigation has been now extended to the reactivity of L coordinated on $\text{Pd}^{\text{II}}\text{P}_2$ ($\text{P}_2 = (\text{PPh}_3)_2, (\text{PEt}_3)_2, \text{dppm}, \text{and dppe}$). The experimental conditions of the demethylation of L on palladium are discussed and compared to those observed with the platinum analogues. To provide a detailed picture of the S–CH₃ bond activation mechanism in these thiolate complexes, various possible mechanistic pathways

Scheme 2. Synthesis of Complexes 1–4

Table 1. Comparison of the M–P and M–S Bond Lengths (Å) as Well as the Thiomethyl ^1H NMR Chemical Shift of $\text{M}(\text{PR}_3)(\eta^1\text{-L})(\eta^2\text{-L})$ Complexes (M = Pd and Pt)

compound	M–P	M–S _{thiolate}	M–S _{thioether}	δ_{CH_3} (ppm) ^a
$\text{Pd}(\text{PEt}_3)(\eta^1\text{-L})(\eta^2\text{-L})$ (1)	2.2746(14)	2.3179(13) 2.3290(13)	2.3602(13)	2.66
$\text{Pt}(\text{PEt}_3)(\eta^1\text{-L})(\eta^2\text{-L})$ ¹¹	2.2593(11)	2.3052(10) 2.3278(10)	2.3418(10)	2.68
$\text{Pd}(\text{PPh}_3)(\eta^1\text{-L})(\eta^2\text{-L})$ (2) ^b	2.2605(9)	2.2978(5) 2.3449(5)	2.3489(5)	2.61
	2.2663(5)	2.3040(5) 2.3441(5)	2.3355(5)	
$\text{Pt}(\text{PPh}_3)(\eta^1\text{-L})(\eta^2\text{-L})$ ^{11b}	2.2459(10)	2.2892(9) 2.3379(9)	2.3303(9)	2.60
	2.2504(10)	2.2937(9) 2.3359(9)	2.3217(9)	

^aAt 295 K. ^bTwo independent molecules in the unit cell.

have been explored by density functional theory (DFT) (B3LYP), and the influence of phosphines (labile or chelating) has been assessed in order to examine the impact onto the privileged pathway of this S–CH₃ bond activation (nucleophilic substitution/addition mechanisms or oxidative addition/reductive elimination sequence). The influence of the coligand has also been evidenced experimentally with the formation of L–L disulfide dimer obtained by reaction of L with MCl_2 (M = Pt and Pd). Note that the reactivity of the *dmit* dithiolene skeleton has been extensively studied¹³ due to the applications of these systems in conducting materials.¹⁴

RESULTS AND DISCUSSION

Reactivity of L toward $\text{Pd}(\text{PR}_3)_2\text{Cl}_2$ and $\text{Pd}(\text{P}(\text{O})\text{P})\text{Cl}_2$ Precursors. The reaction of *cis*- $\text{Pd}(\text{PR}_3)_2\text{Cl}_2$ ($\text{PR}_3 = \text{PEt}_3$ and PPh_3) with 2 equiv of CsL in refluxing MeOH afforded as main products complexes $\text{Pd}(\text{PR}_3)(\eta^1\text{-L})(\eta^2\text{-L})$ (R = Et: 1; R = Ph: 2) in moderate yields (~60%). Using the procedure reported by Olk and co-workers for the synthesis of $\text{Pd}(\text{dppe})(\eta^1\text{-L})_2$ (3) (dppe = 1,2-bis(diphenylphosphanyl)ethane),¹⁵ chelate compound $\text{Pd}(\text{dppm})(\eta^1\text{-L})_2$ (4) has been synthesized in 75% yield as a red solid (Scheme 2).

These complexes are highly soluble in chlorinated solvents but poorly soluble in MeOH. The ^1H NMR spectra of 1 and 2 reveal the presence of two sulfur-rich ligands for one phosphine

and consequently the substitution of one phosphine by a thiomethyl group. In all these complexes, the hydrogen atoms of the thiomethyl groups appear at room temperature as a singlet. The resonances displayed by 1 (2.66 ppm) and 2 (2.61 ppm) are downfield-shifted with respect to the signals observed in 3 (2.25 ppm) and $\text{Pd}(\eta^2\text{-dppm})(\eta^1\text{-L})_2$ (2.40 ppm). Thus, the dative S(thioether) → Pd interaction in 1 and 2 exchanges swiftly in solution between the thiomethyl groups of the two sulfur ligands present in the coordination sphere of the metal. This behavior is identical to that observed in the analogues platinum complexes which exhibit quite the same chemical shifts for the hydrogen atoms of L (Table 1).¹⁶ However, whereas the nonequivalence of the thiomethyl groups was established below 240 K in the ^1H NMR spectra of the Pt(II) complexes, the freezing of the dynamic exchange requires much more lower temperature with the Pd(II) complexes. Using CD_2Cl_2 as solvent, the coalescence temperature was estimated near the freezing point of CD_2Cl_2 (173 K). This result is in accordance with the well-established effect of the central metal ion on the rate of square planar substitutions.¹⁷ The molecular structures of $\text{Pd}(\text{Et}_3)(\eta^1\text{-L})(\eta^2\text{-L})$ and $\text{Pd}(\text{PPh}_3)(\eta^1\text{-L})(\eta^2\text{-L})$ were determined by single crystal X-ray diffraction studies. $\text{Pd}(\text{PEt}_3)(\eta^1\text{-L})(\eta^2\text{-L})$ crystallizes in the monoclinic system and space group $P2_1/c$ (Figure 1). $\text{Pd}(\text{PPh}_3)(\eta^1\text{-L})(\eta^2\text{-L})$ crystallizes in the triclinic system and space group $P\bar{1}$, with two

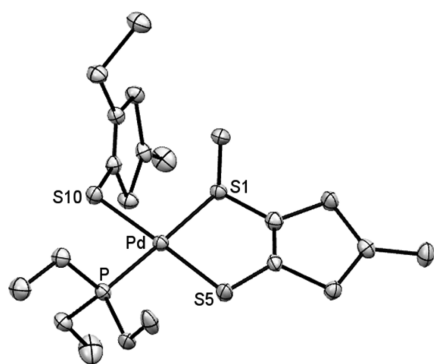


Figure 1. ORTEP diagram (50% probability level) of **1**. H atoms are omitted for clarity. Selected bond lengths [Å] and angles [deg]: Pd–P 2.2746(14), Pd–S(5) 2.3179(13), Pd–S(1) 2.3602(13), Pd–S(10) 2.3290(13), P–Pd–S(5) 91.99(5), P–Pd–S(1) 178.20(5), P–Pd–S(10) 85.71(4), S(5)–Pd–S(1) 89.60(4), S(5)–Pd–S(10) 177.61(5), S(1)–Pd–S(10) 92.71(4).

independent complexes and one CHCl_3 molecule in a general position in the unit cell (Figure 2). In both complexes, the Pd

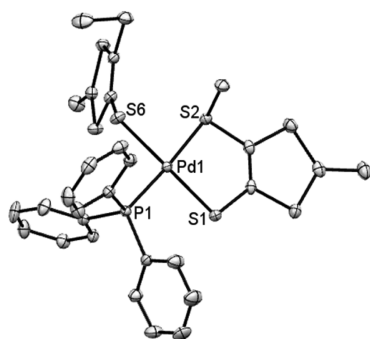


Figure 2. ORTEP diagram (50% probability level) of **2**. H atoms and solvent molecules are omitted for clarity. Only one of the two independent molecules in the unit cell is depicted. Selected bond lengths [Å] and angles [deg] {equivalent values measured for the second independent molecule in the unit cell}: Pd(1)–P(1) 2.2605(5) {2.2663(5)}, Pd(1)–S(1) 2.2978(5) {2.3040(5)}, Pd(1)–S(2) 2.3489(5) {2.3355(5)}, Pd(1)–S(6) 2.3449(5) {2.3441(5)}, P–Pd(1)–S(1) 92.453(18) {91.348(18)}, P–Pd(1)–S(2) 175.945(19) {175.033(19)}, P–Pd(1)–S(6) 86.615(19) {89.83(2)}, S(1)–Pd(1)–S(2) 90.821(18) {90.453(18)}, S(1)–Pd(1)–S(6) 178.486(19) {177.891(19)}, S(2)–Pd(1)–S(6) 90.161(19) {88.230(19)}.

atom displays a slightly distorted square-planar coordination with cis angles in the range of 85.65–92.77° and 86.62–92.45° for **1** and **2**, respectively. The Pd– S_{thiolate} distances (2.317 and 2.329 Å for **1**; 2.297, 2.304, 2.344, and 2.344 Å for **2**) are similar to those reported for other Pd– S_{thiolate} bonds,^{8a,17} but of note is that they are shorter than those measured in the Pd(dppe)(η^1 -L)₂ complex (2.385 and 2.375 Å).¹⁵ This observation is in agreement with the greater thermodynamic trans influence of phosphine compared to that of thiolate ligand. In the Pd(η^2 -L)-metallacycle, the Pd– $S_{\text{thioether}}$ bond length is, as expected, significantly longer than the Pd– S_{thiolate} one given the different charges of the donor atoms. Note however that in compound **2** the Pd– $S_{\text{thioether}}$ distance is comparable to the Pd– S_{thiolate} bond length of the Pd(η^1 -L) fragment. The metric parameters of these palladium complexes are comparable to those of the platinum analogues (Table 1) with the M–L distances being slightly longer, in agreement

with the values of covalent radii (1.39 Å for Pd and 1.36 Å for Pt).¹⁸

Lability of the Phosphine Group. The reactivity of L on *cis*-[MP₂Cl₂] (M = Pd and Pt) is sensitive to the nature of the metal in function of the lability of the phosphine. This latter is higher in the case of palladium complexes. Whereas the bis(thiolate) *trans*-Pt(PEt₃)₂(η^1 -L)₂ is the main product obtained by reaction at room temperature of 2 equiv of L with *cis*-Pt(PEt₃)₂Cl₂,¹¹ the presence of Pd(PEt₃)₂(η^1 -L)₂ is identified only as a minor product in the NMR spectra (δ = 16.6 ppm in the ³¹P{¹H} NMR and δ = 2.48 ppm for the SMe groups in the ¹H NMR) of the crude product obtained by reaction of 2 equiv of L with *cis*-Pd(PEt₃)₂Cl₂. As previously described, the major species is [Pd(PEt₃)(η^1 -L)(η^2 -L)] (**1**). The evolution of M(PEt₃)₂(η^1 -L)₂ toward M(PEt₃)(η^1 -L)(η^2 -L) seems not driven by the strength of the M– $S_{\text{thiomethyl}}$ interaction since the thiomethyl ¹H NMR chemical shifts are very close in the respective Pd and Pt complexes (Table 1). With Pd(PPh₃)₂Cl₂ as starting material, Pd(PPh₃)(η^1 -L)(η^2 -L) (**2**) is the single complex identified in the NMR spectra when performing the reaction in refluxing MeOH. Addition of 1 equiv of PPh₃ to a toluene-*d*₈ solution of **2** leads to broad peaks centered at 32.6 ppm (**2**) and –5 ppm (PPh₃) in the ³¹P{¹H} NMR spectrum, whereas no change is observed in the ¹H NMR spectrum (except the increase of the intensity of the signals in the aromatic range). At 363 K, the exchange between coordinated and free PPh₃ (according to the equilibrium Pd(PPh₃)(η^1 -L)(η^2 -L) + *PPh₃ ⇌ Pd(*PPh₃)(η^1 -L)(η^2 -L) + PPh₃) is sufficiently fast so that only one “averaged” entity is observed as a very broad hump. Thus, the dissociation of the triphenylphosphine ligand of complex **2** is also facile. The absence of formation of Pd(PPh₃)₂(η^1 -L)₂ by addition of PPh₃ on **2** is also shown by UV–visible experiments since **2** shows transitions at 311 and 416 nm which are insensitive to the addition of an excess of triphenylphosphine (Figure S1). At 363 K, a toluene-*d*₈ solution of **2** exhibits very broad peaks in the ¹H and ³¹P{¹H} NMR spectra (Figure 3). These observations may indicate that the equilibrium Pd(PPh₃)(η^1 -L)(η^2 -L) ⇌ Pd(η^2 -L)₂ + PPh₃ exists in solution at high temperature.

The higher phosphine lability in palladium complexes was also noticed with the diphosphine dpmm ligand. Whereas Pt(η^2 -dpmm)(η^1 -L)₂ is rigid in solution, an equilibrium between Pd(η^2 -dpmm)(η^1 -L)₂ and the coordination isomer Pd(η^1 -dpmm)(η^1 -L)(η^2 -L) is observed in solution (Scheme 2). In the ³¹P{¹H} NMR spectrum at 295 K (Figure 4), the chelating dpmm ligand gives rise to a broad singlet at –38.3 ppm,^{17a,19} and the dangling dpmm is characterized by two broad signals centered at 27.5 ppm (–Ph₂P–Pd) and –23.2 ppm (–CH₂–PPh₂).^{17a,20} Note that the thiomethyl protons of Pd(η^1 -dpmm)(η^1 -L)(η^2 -L) appear at room temperature as a singlet at 2.58 ppm suggesting that a dynamic η^1 -L/ η^2 -L exchange occurs at room temperature. From the NMR spectra, the Pd(η^2 -dpmm)(η^1 -L)₂/Pd(η^1 -dpmm)(η^1 -L)(η^2 -L) ratio can be estimated to be 9:1 at 293 K. In contrast, the five-membered metallacycle Pd(η^2 -dppe) seems not to be hemilabile in solution since only one sharp singlet at 59.6 ppm is observed in the ³¹P{¹H} NMR spectrum corresponding to compound **3**. No trace of Pd(η^1 -dppe)(η^1 -L)(η^2 -L) is detected by NMR. It is noteworthy that dissociation of one M–P bond in complexes **1**, **2**, and **4** is induced by an intramolecular interaction between a thiomethyl group and the metal. For MP₂(dithiolene) complexes, such phosphine dissociation is sometimes observed but intermolecular M⋯S interactions generating dimetallic

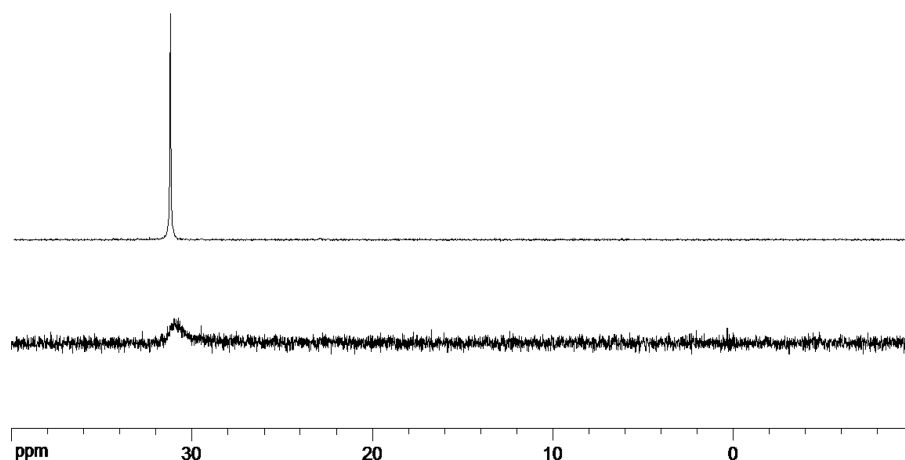


Figure 3. $^{31}\text{P}\{^1\text{H}\}$ of $\text{Pd}(\text{PPh}_3)(\eta^1\text{-L})(\eta^2\text{-L})$ (**2**) in $\text{toluene-}d_8$ at 298 K (top) and 363 K (bottom).

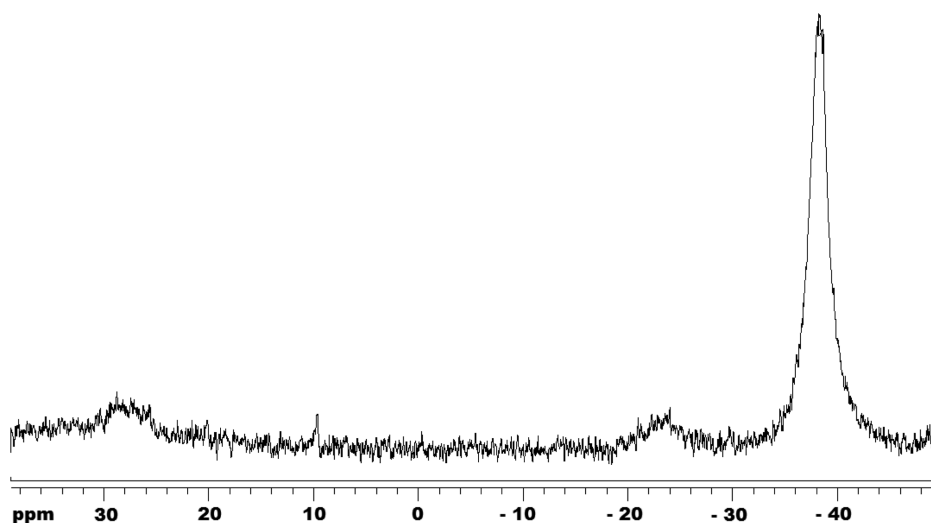
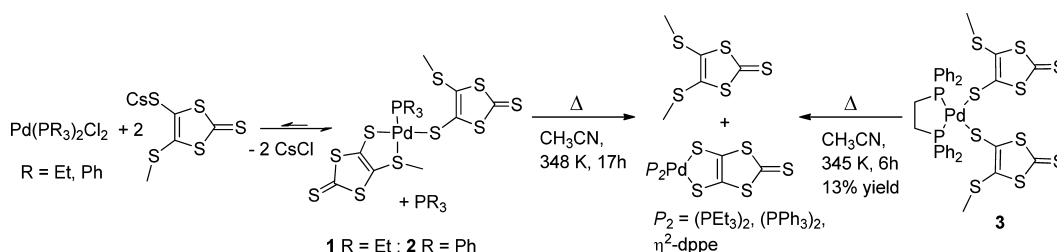


Figure 4. $^{31}\text{P}\{^1\text{H}\}$ spectrum at 295 K of a CDCl_3 solution of $\text{Pd}(\text{dppm})(\text{L})_2$ (**4**).

Scheme 3. Demethylation Reactions Affording Dithiolene Complexes



species $[\text{MP}(\mu\text{-dithiolene})_2]$ appear to be the driving force in this case.²¹

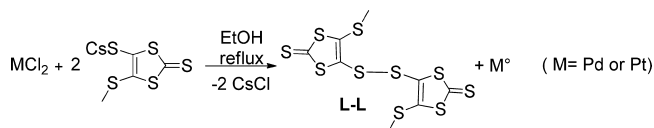
Demethylation Reaction. The L ligand coordinated on Pd is also prone to demethylation (Scheme 3). Indeed, NMR spectroscopy revealed a partial evolution (13% yield) of bis(thiolate) compound **3** to the dithiolene complex $\text{Pd}(\eta^2\text{-dppm})(\text{dmit})$ ($\delta = 56.7$ ppm in the $^{31}\text{P}\{^1\text{H}\}$ NMR) and concomitant formation of Me_2dmit ($\delta = 2.49$ ppm in the ^1H NMR) after heating in acetonitrile at 345 K for 6 h. Under the same conditions, a demethylation rate of 82% has been determined for the Pt derivative, whereas dppm-ligated Pd complex **4** was reluctant to demethylate. The formation of $\text{Pd}(\eta^2\text{-dppm})(\text{dmit})$ ($\delta = -39.0$ ppm in the ^{31}P NMR) and

Me_2dmit however takes place when a solution of **4** in DMF is heated at 403 K for 6 h. In addition, for comparison we reacted $\text{Pd}(\text{PR}_3)_2\text{Cl}_2$ and $\text{Pt}(\text{PR}_3)_2\text{Cl}_2$ ($\text{R} = \text{PEt}_3$ and PPh_3) with 2 equiv of CsL in acetonitrile at 345 K for 17 h. Analysis of the reaction mixtures revealed a $\text{M}(\text{PR}_3)_2(\text{dmit})/\text{M}(\text{PR}_3)(\eta^1\text{-L})(\eta^2\text{-L})$ ratio of 100/0 for $\text{M} = \text{Pt}$ and $\text{R} = \text{Ph}$, 80/20 for $\text{M} = \text{Pt}$ and $\text{R} = \text{Et}$, 40/60 for $\text{M} = \text{Pd}$ and $\text{R} = \text{Et}$, and 5/95 for $\text{M} = \text{Pd}$ and $\text{R} = \text{PPh}_3$. It should be stressed that in both of these Pd and Pt complexes the thermally induced demethylation occurs without the presence of an external nucleophile, contrasting with the reactivity pattern depicted in Scheme 1b,d.

Reactivity toward MCl_2 ($\text{M} = \text{Pd}$ and Pt). Two equivalents of CsL were also reacted with MCl_2 ($\text{M} = \text{Pd}$

and Pt) in refluxing ethanol. *A priori*, this reaction might lead to $M(\eta^2-L)_2$ species identified as thermodynamically stable molecule in the theoretical study (see below). After separation of a black powder, the workup of the filtrate afforded the L–L dimer as an orange microcrystalline solid in low yield (Scheme 4). This disulfide, soluble in halogenated solvents, is stable at

Scheme 4. Synthesis of L–L



ambient temperature. Spectroscopic characterizations reveal only one singlet at 2.55 ppm in the 1H NMR spectrum and a strong absorption at 1061 cm^{-1} in the IR spectrum, associated with the presence of a C=S bond. The Raman spectrum recorded in CH_2Cl_2 solution shows two bands in the S–S stretching region situated at 460 and 508 cm^{-1} .²² The presence of two bands may result from the coexistence of two rotamers in solution differing from the relative conformation, *cis* or *trans*, of the C_α atoms linked by a disulfide bridge.

The molecular structure of L–L was determined by X-ray diffraction. The molecule is symmetric with a C_2 axis perpendicular to the S–S bond which inverts the two L units (Figure 5). The S–S bond distance of $2.0929(11)\text{ \AA}$ is slightly shorter than those reported for the dianions $C_6S_{10}^{2-}$ featuring two *dmit* units linked by one S–S bond ($2.135(4)\text{ \AA}$) and $C_{12}S_{16}^{2-}$ in which two 1,3-dithiole-2-thione rings are also connected by one disulfide bond ($2.157(12)\text{ \AA}$).²³ The S–S separation in L–L is similar to the value of $2.0757(9)\text{ \AA}$ observed in the rigid molecular C_6S_{10} compound whose structure consists in two *dmit* units linked by two disulfide bonds.²⁴ The torsion angle of 101.3° measured by the dihedral angle of the C–S–S–C linkage is usual. The stabilization arising from dihedral angles near 90° has been explained by the overlap of one σ^*_{S-C} orbital and the 3p lone pair located on the other sulfur atom which is maximized in such a conformation.²⁵ In contrast to the compound described here, the dianion $C_6S_{10}^{2-}$ does not follow this general rule since an unusually acute dihedral angle of 51.9° was reported.²³ In this case, the twist was not favorable for hyperconjugation but allows intramolecular $\pi-\pi$ interactions between the 1,3-dithiole-2-thione cores. For L–L, the dihedral angle of 101.3° is not consistent with intramolecular π stacking, but the packing diagram in the solid state exhibits intermolecular $\pi-\pi$ interactions with separation of the 1,3-dithiole-2-thione rings of 3.49 \AA (Figure 5).

Due to the cost and the stoichiometric need of $PtCl_2$ or $PdCl_2$ in the reaction described above, we investigated an alternative method to synthesize dimer L–L. The oxidative coupling of thiols to disulfide has been extensively studied, and besides protocols using iodine or air as oxidizing agents, a wide range of methods have been developed.²⁶ An efficient and mild procedure involving 1 equiv of hydrogen peroxide and a catalytic amount of iodide has been recently reported.²⁷ Using this method, dimer L–L was synthesized in 40% yield starting with the CsL thiolate dissolved in water. L–L reacts in $CDCl_3$ by oxidative addition across 1 equiv of the zero-valent $Pt(PPh_3)_2(PhC\equiv CPh)$ complex to afford as product $[Pt(PPh_3)(\eta^1-L)(\eta^2-L)]$ identified on the basis of its NMR spectroscopic data.¹¹ This reactivity is similar to that observed between tetrathiocenes and zero-valent group 10 transition metal complexes yielding dithiolate complexes.²⁸

We also examined the reactivity of 2 equiv of CsL toward $M^{II}(cod)Cl_2$ ($M = Pd$ and Pt , *cod* = 1,5-cyclooctadiene) in refluxing ethanol. In both cases, only insoluble products have been isolated. The presence of the *dmit* core was evidenced in the IR spectra by the signature of the C=S bond near 1050 cm^{-1} . No *cod* could be detected in the IR spectra of the solids. Elemental analyses indicated a S/C ratio close to 3 in accordance with the presence of L in this insoluble material. A similar result was obtained after reaction of CsL with $Pd(SET)_2Cl_2$. Due to the very low solubility of the isolated products, it was not possible to obtain information from NMR spectroscopy, so at this stage, it would be speculative to conclude on the structure of these compounds. Nevertheless, these experiences point out the influence of the ancillary ligand on the reactivity of L toward Pd^{II} and Pt^{II} .

Theoretical Study. To gain more insight into the mechanism of the C–S bond activation and the influence of the phosphine ligands on the nature of the privileged pathway, DFT calculations were carried out at the B3LYP/SMD(CH_3CN)/SDD+f(M),6-31G** (other atoms)//B3LYP/SDD+f(M),6-31G** (other atoms) level of theory (see the Computational Details section). The solvent effect (CH_3CN) was taken into account by the SMD solvation model. We examined two specific cases involving either a labile phosphine, PEt_3 or PPh_3 , for which the intermediates $M(PR_3)(\eta^1-L)(\eta^2-L)$ have been experimentally isolated and characterized, or a chelate phosphine (*dppe*), where no occurrence of $M(\eta^1-dppe)(\eta^1-L)(\eta^2-L)$ complex was observed by NMR spectroscopy.

For labile phosphines PEt_3 and PPh_3 , the starting point of the theoretical study was complex $M(PR_3)_2(\eta^1-L)_2$, identified as minor product when $Pd(PEt_3)_2Cl_2$ was reacted with two equiv of L and major product when using $Pt(PEt_3)_2Cl_2$. The latter

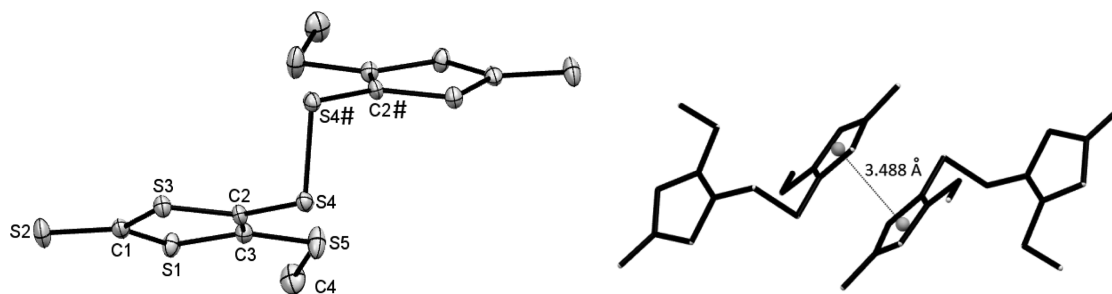
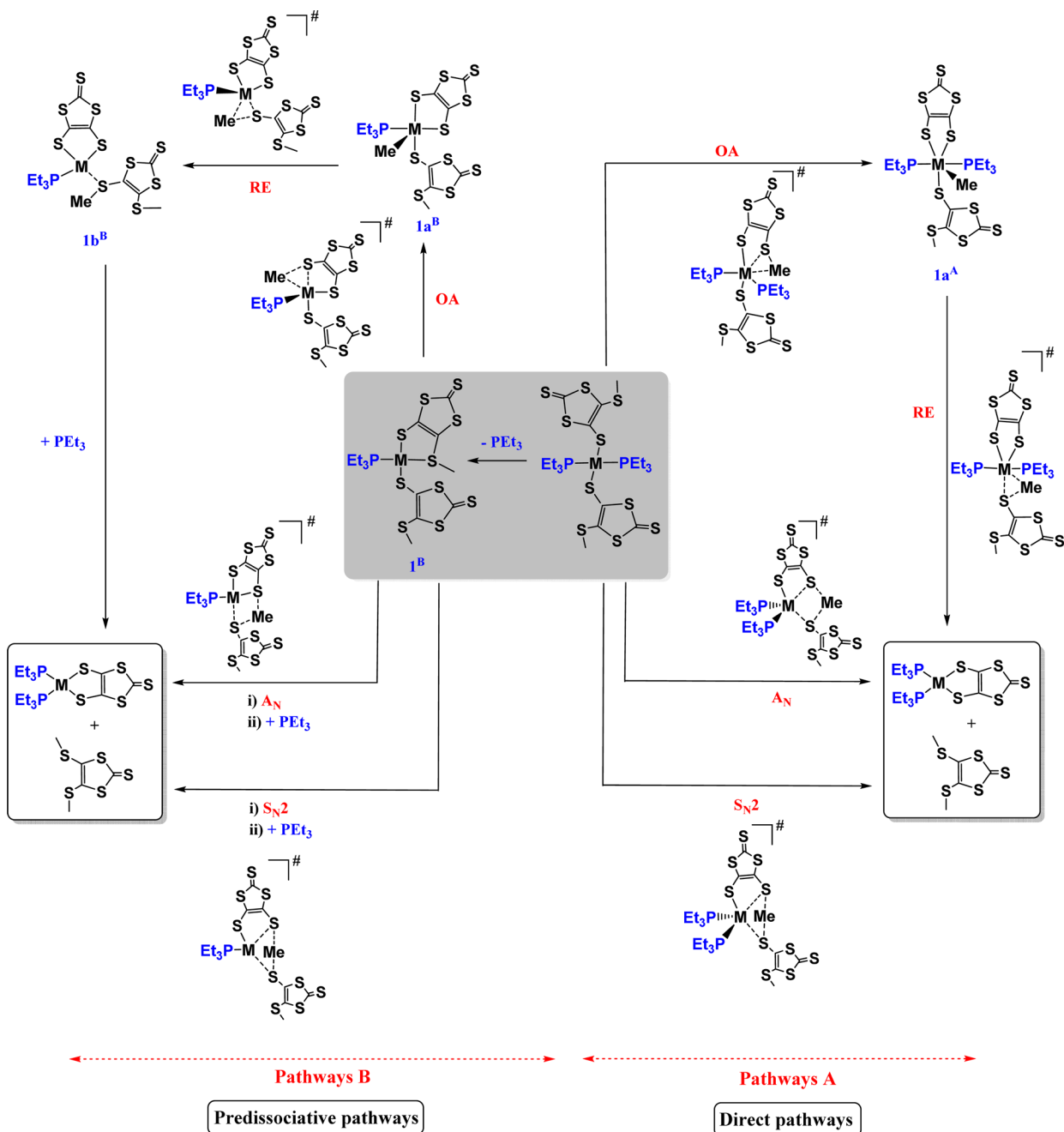


Figure 5. ORTEP diagram (50% probability level) of L–L (left) and view of the intermolecular $\pi-\pi$ interactions in the solid state (right). Symmetry transformations to generate equivalent atoms: #, $-x + 1, y, -z + 1/2$.

Scheme 5. Plausible Mechanisms for C–S Bond Activation in $trans\text{-M}^{\text{II}}(\text{PEt}_3)_2(\eta^1\text{-L})_2$ Complex^a

^aIncluding oxidative addition/reductive elimination sequence, nucleophilic substitution $S_{\text{N}}2$, and nucleophilic addition A_{N} . Pathways A correspond to direct pathways, and pathways B to pathways involve phosphine predissociation.

can undergo direct demethylation or demethylation after predissociation of one phosphine ligand through complex $\text{M}(\text{PR}_3)(\eta^1\text{-L})(\eta^2\text{-L})$. From model complex $\text{Pd}^{\text{II}}(\text{PEt}_3)_2(\eta^1\text{-L})_2$ and its analogue with aryl groups $\text{Pd}^{\text{II}}(\text{PPh}_3)_2(\eta^1\text{-L})_2$, two isomers have been localized on the potential energy surface (PES), according to the position of the phosphine groups (cis or trans). $trans\text{-Pd}(\text{PR}_3)_2(\eta^1\text{-L})_2$ was found to be around 5.6 kcal/mol (PEt_3)/9.2 kcal/mol (PPh_3) more stable than $cis\text{-Pd}(\text{PR}_3)_2(\eta^1\text{-L})_2$. Similar results have been obtained for the platinum complexes, with an energy difference of around 4.1 kcal/mol (PEt_3)/9.3 kcal/mol (PPh_3). The privileged trans configuration is in agreement with experimental observations since the unique formation of $trans\text{-}[\text{Pt}^{\text{II}}(\text{PR}_3)_2(\eta^1\text{-L})_2]$ has

been previously ascertained by the magnitude of NMR J_{PtP} coupling constants and X-ray structures.¹¹ Moreover, a survey of structurally characterized PtP_2S_2 complexes has shown that the trans configuration is the more common arrangement with monodentate ligands.²⁹ These theoretical data suggest a poor probability of having the cis isomer in the mixture, according to the Maxwell–Boltzmann distribution. Consequently, we focused calculations on the reactivity of $trans\text{-M}^{\text{II}}(\text{PR}_3)_2(\eta^1\text{-L})_2$ complexes and analyzed the different plausible mechanisms for the C–S bond activation.

Case of Labile Phosphine PEt_3 . To rationalize the formation of square planar dithiolene complex $\text{M}^{\text{II}}(\text{PEt}_3)_2(\text{dmit})$, we supposed several mechanistic scenarios (Scheme 5): (i)

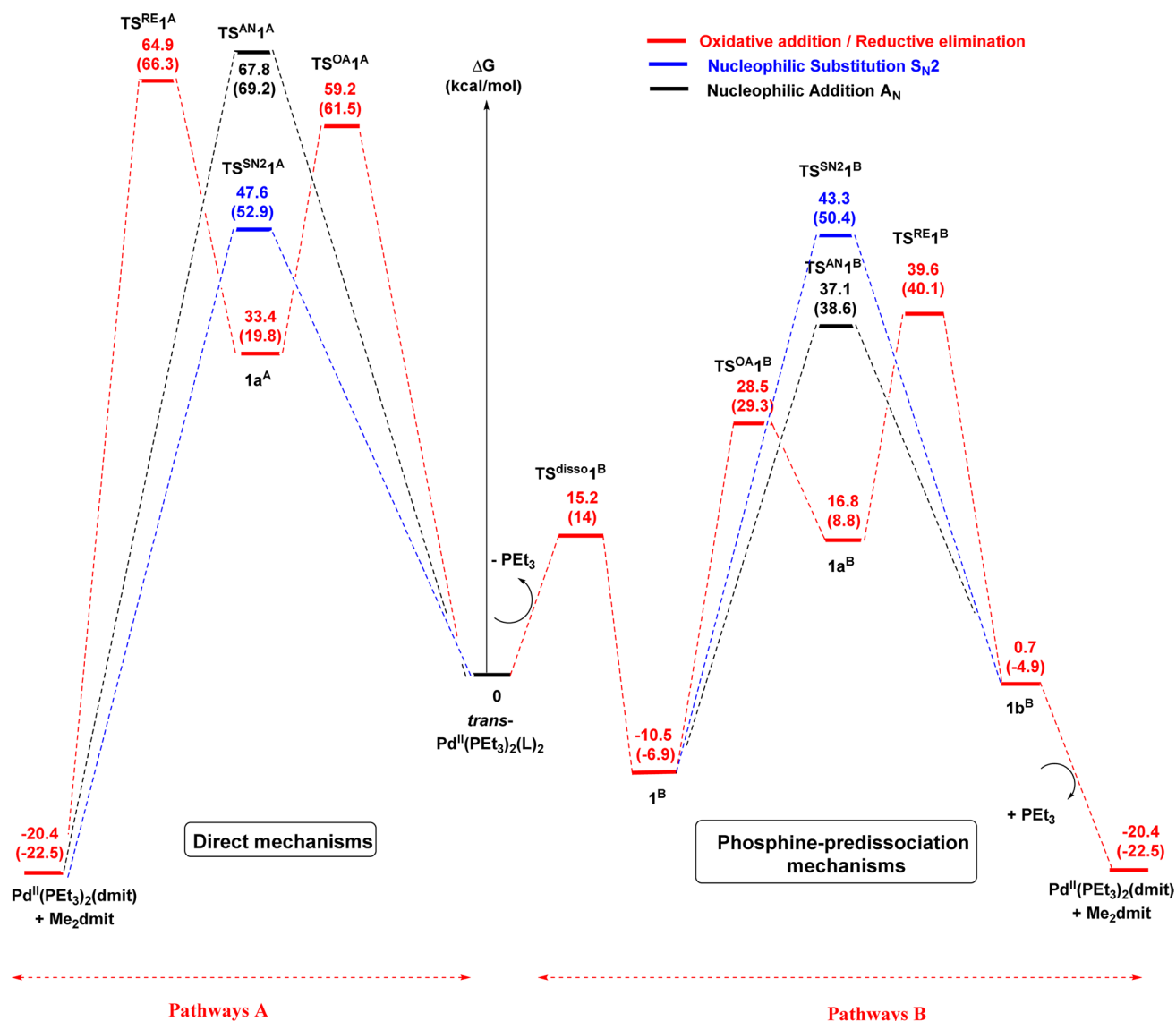


Figure 6. Energy profiles ($\Delta G^{\text{CH}_3\text{CN}}$ in kcal/mol) for direct mechanisms (pathways A) and phosphine-predissociation mechanisms (pathways B) for C–S bond activation in *trans*-Pd^{II}(PEt₃)₂(η¹-L)₂ complex, calculated at the B3LYP/SMD(CH₃CN)/SDD+f(M),6-31G** (other atoms)//B3LYP/SDD+f(M),6-31G** (other atoms) level of theory. The values in parentheses correspond to the results for the corresponding *trans*-Pt^{II}(PEt₃)₂(η¹-L)₂ complex.³⁰

Pathways A: Direct mechanisms from *trans*-M(PEt₃)₂(η¹-L)₂ complex with the two alkylphosphines coordinated to the metal center throughout the entire process. Three different pathways have been considered: (path A-OA/RE) This is a two-step process with oxidative addition of the S–C_{Me} bond to M(II) leading to M^{IV}(PEt₃)₂(η¹-L)(dmit)Me intermediate (1a^A), which can convert by reductive elimination of Me₂dmit to M^{II}(PEt₃)₂(dmit). This intermediate adopts an octahedral geometry with the two phosphine ligands at the axial position of the square plane formed by methyl group and the three sulfur atoms and may be related to the octahedral Pt^{IV}(PMe₃)₂(dithiolene)₂ complexes, recently described by Donahue et al.^{21a} (path A-S_N2) This pathway corresponds to an intramolecular concerted S_N2 reaction with a thiolate sulfur atom acting as the nucleophile and M^{II}(PEt₃)₂(dmit) complex being the leaving group. The nucleophile approaches the thiomethyl group at an angle of 180° with respect to the C_{CH₃}–S bond, thus providing the optimal overlap between the sulfur

lone pair (n_{S2}) and the σ*_{S3–CH₃} orbital. At the transition state, the S-partially bonded carbon adopts a trigonal bipyramidal geometry with S2 and S3 atoms in axial position. (path A-A_N) In this pathway, the C–S bond activation proceeds through a transition state involving a CH₃⁺ carbocation equidistant to the S_{thiolate} and S_{thioether} atoms. The sulfur lone pair (p character) of the thiolate S₂ atom and the 2pπ(C) orbital of the carbocation are correctly oriented to interact, favoring a nucleophilic attack. For simplicity, this mechanism will be named hereafter nucleophilic addition (A_N). (ii) Pathways B: Mechanisms involving one phosphine predissociation from *trans*-M(PEt₃)₂(η¹-L)₂ complex. The intramolecular substitution of one PEt₃ ligand by the thiomethyl group SMe affords the square planar species M^{II}(PEt₃)₂(η¹-L)(η²-L) (1^B). As previously described, several pathways can take place from this intermediate: (path B-OA/RE) This is a multistep process implying an oxidative addition/reductive elimination sequence followed by phosphine recoordination. The penta-coordinated

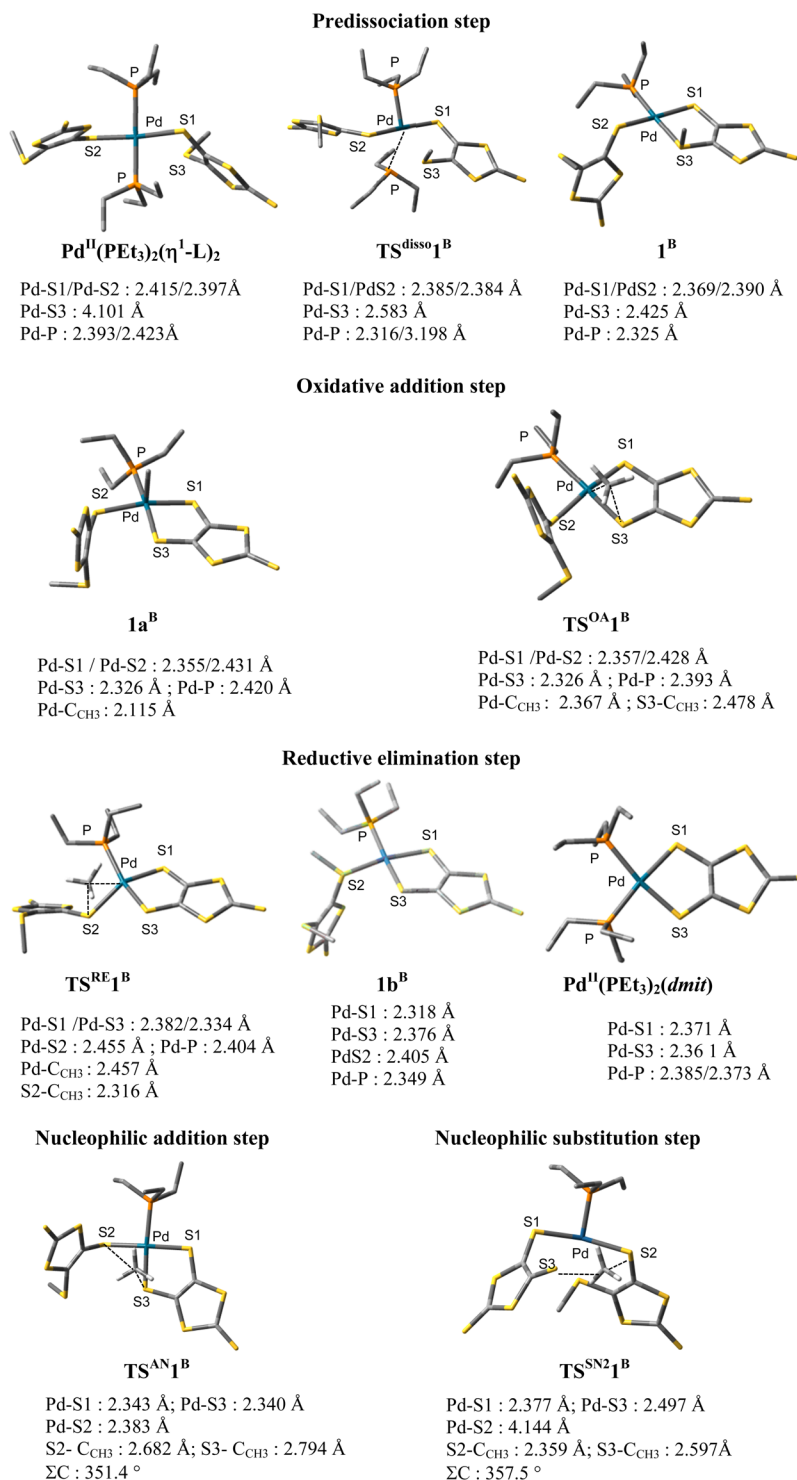


Figure 7. Main minima and TS involved in the phosphine-predissociation mechanisms: oxidative addition/reductive elimination sequence (path B-OA/RE), nucleophilic addition (path B-A_N), and S_N2 reaction (path B-S_N2) from *trans*-Pd^{II}(PEt₃)₂(η¹-L)₂ complex.

oxidative addition product M^{IV}(PEt₃)(η¹-L)(*dmit*)Me (**1a^B**) can be described as a square pyramidal with the methyl group perpendicular to the square plane occupied by the P and the three S atoms. This latter can then undergo reductive elimination of the C–S_{thioether} bond and finally form M^{II}(PEt₃)₂(*dmit*) after recoordination of PEt₃. (paths B-S_N2 and B-A_N) These correspond to the S_N2 and nucleophilic addition (A_N) mechanisms from M^{II}(PEt₃)(η¹-L)(η²-L) species.

For the sake of clarity, only the most plausible mechanisms will be described in detail hereafter. According to DFT calculations, all energy profiles involving direct pathways (pathways A, Scheme 5) can be ruled out because the transition states (TS's) lie 47.6 to 64.9 above the reactant *trans*-Pd^{II}(PEt₃)₂(η¹-L)₂ (Figure 6).³⁰ In agreement with the experimental observations, theoretical results (Figures 6 and 7) point out that the formation of Pd^{II}(PEt₃)(η¹-L)(η²-L) (**1^B**) is kinetically and thermodynamically favored [$\Delta G^\ddagger(\text{TS}^{\text{disso}}1^{\text{B}}) =$

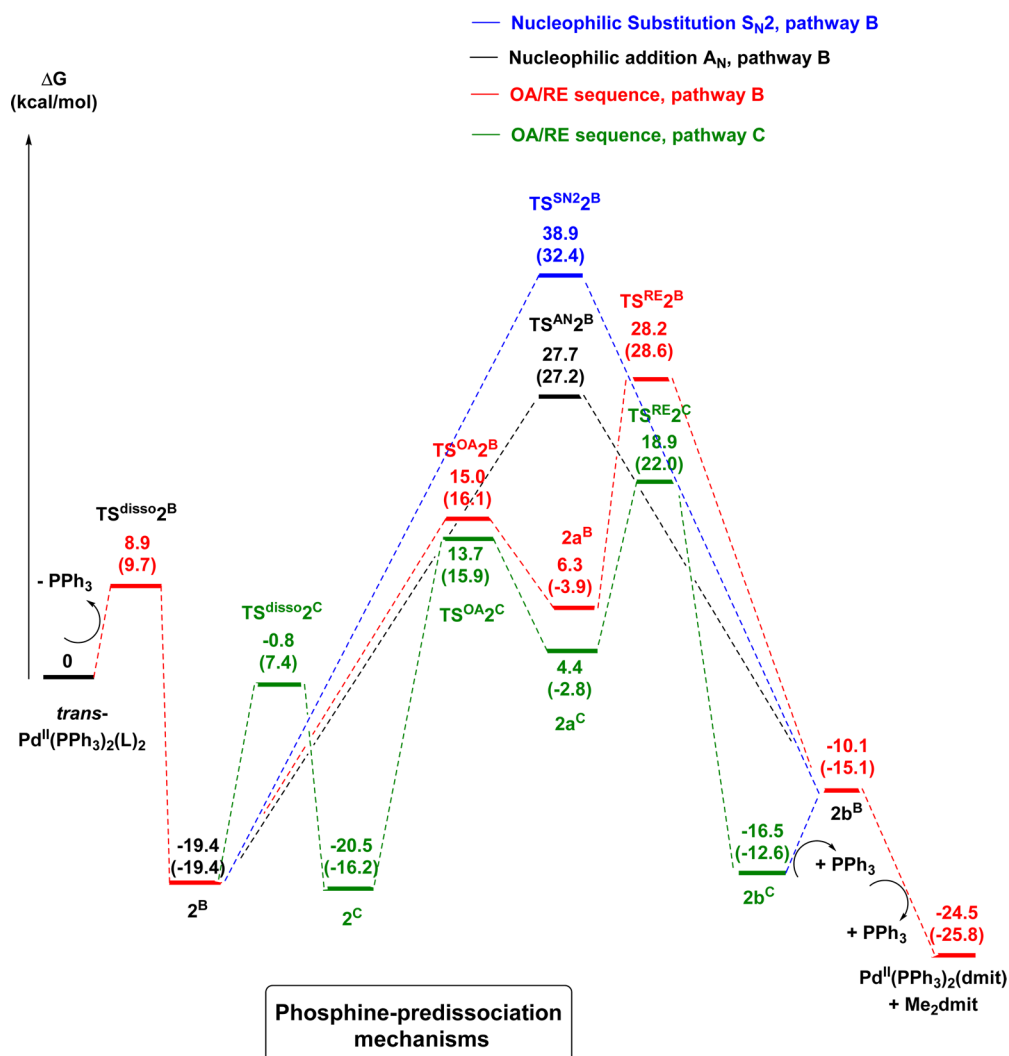


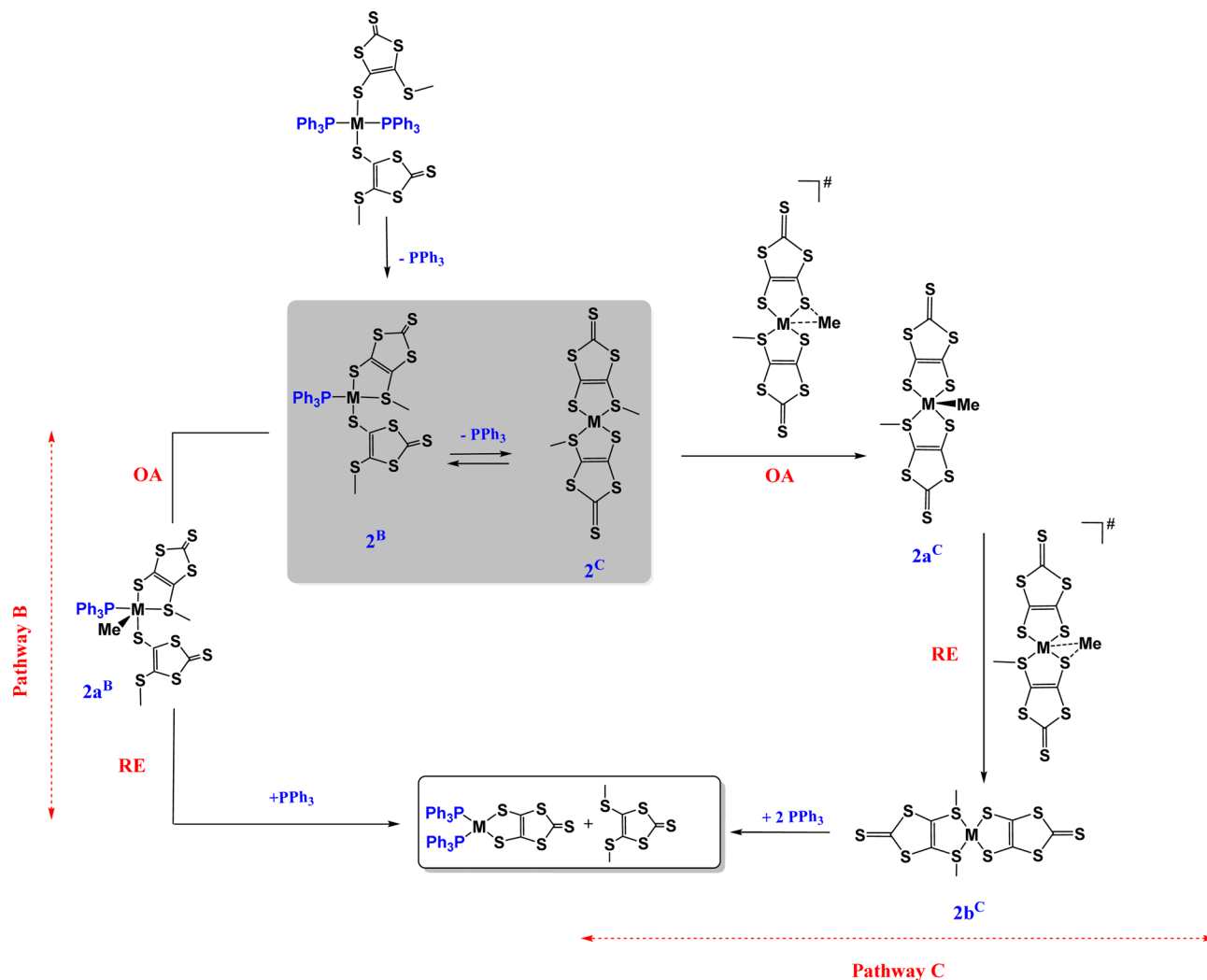
Figure 8. Energy profiles (ΔG^{CH_3CN} in kcal/mol) for C–S bond activation from $trans-Pd^{II}(PPh_3)_2(\eta^1-L)_2$ calculated at the B3LYP/SMD(CH_3CN)/SDD+f(M),6-31G** (other atoms)//B3LYP/SDD+f(M),6-31G** (other atoms) level of theory and involving the phosphine-predissociation pathways B and C: (a) oxidative addition/reductive elimination sequence through 2^B , in red (B-OA/RE), (b) nucleophilic addition through 2^B , in black (B- A_N), (c) S_N2 pathway (B- S_N2) through 2^B , in blue, and (d) oxidative addition/reductive elimination sequence through 2^C , in green (C-OA/RE). The values in parentheses correspond to the results for the analogue $trans-Pt^{II}(PPh_3)_2(\eta^1-L)_2$ complex.³⁴

15.2 kcal/mol and $\Delta G(trans-Pd^{II}(PEt_3)_2(\eta^1-L)_2 \rightarrow I^B) = -10.5$ kcal/mol].³¹ This step proceeds through a concerted dissociative mechanism with a late TS featuring dissymmetric P–Pd distances (2.316 and 3.198 Å), short Pd–S1/Pd–S2 bond lengths (2.385/2.384 Å), and a quasi-formed Pd–S3 bond (2.583 Å), only elongated around by 0.2 Å compared to Pd–S1/Pd–S2 ones.

In light of these theoretical data, we have explored more specifically the three dissociative mechanisms (B-OA/RE, B- S_N2 , and B- A_N) involving tetra-coordinated square planar intermediate I^B , which is stabilized by a strong coordination of the thiomethyl group to the metal center [Pd–S3(Me): 2.425 Å, close to Pd–S1/PdS2: 2.369–2.390 Å, NBO analysis: LP1(S3) \rightarrow Pd: 8.6 kcal/mol and LP2(S3) \rightarrow Pd: 96.2 kcal/mol, Table S1]. DFT calculations (Figure 6) suggested that the intramolecular S_N2 -like reaction (B- S_N2 , Scheme 5) is the less feasible process. The TS lies at 43.3 kcal/mol ($TS^{SN2}I^B$) above the initial reactant $Pd^{II}(PEt_3)_2(\eta^1-L)_2$. The nucleophilic addition (B- A_N) takes place through an activation barrier ($TS^{AN}I^B$) lower in energy by around 6.2 kcal/mol and is therefore the most privileged pathway. It can also compete with

oxidative addition/reductive elimination sequence (B-OA/RE mechanism) since the rate-determining reductive elimination step appears at almost the same energy as that of A_N process ($TS^{RE}I^B$, 2.5 kcal/mol higher in energy than $TS^{AN}I^B$, Figure 6). However, in the OA/RE sequence, the oxidative addition step, whose activation barrier is lower in energy than reductive elimination by around 10 kcal/mol, can be reversible (penta-coordinate intermediate Ia^B is thermodynamically less stable than I^B by around 27.3 kcal/mol). Consequently, the feasibility of demethylation process through this sequence may be impacted by promoting a competition between reductive elimination of Me_2dmit at palladium (thermodynamic control) leading to the dithiolene complex $Pd^{II}(PEt_3)_2(dmit)$ or a backward reaction giving rise to the regeneration of I^B (kinetic control). The activation barriers of the reductive elimination step and the nucleophilic addition (A_N) mechanism are significant but accessible under the specific experimental conditions (heating at 348 K during 17 h) and may explain why the demethylation process is not effective.

Analysis of the associated transition states (Figure 7) revealed that in the nucleophilic addition process B- A_N , the

Scheme 6. Other Mechanism for C–S Bond Activation (Pathway C) in $M^{II}(PPh_3)_2(\eta^1-L)_2$ Complex^a

^aMechanism involves oxidative addition/reductive elimination sequence and going through $M^{II}(\eta^2-L)_2$ (complex 2^C).

methyl group is quasi-equidistant to S2 and S3 atoms ($C_{CH_3} \cdots S2$: 2.682 Å versus $C_{CH_3} \cdots S3$: 2.794 Å), with a quasi-planar environment of the carbon center (ΣC : 351.4°). The oxidative addition proceeds through a late 3-center transition state involving Pd, S3, and C_{CH_3} atoms. The main geometric features associated with $TS^{OA}1^B$ are a partially formed C_{CH_3} –Pd bond (2.367 Å versus 2.115 Å in $1a^B$), an elongated C_{CH_3} –S3 bond (2.498 Å versus 1.842 Å in 1^B), and a classical Pd–S3 distance (2.367 Å). Likewise, reductive elimination transition state $TS^{RE}1^B$ displays a 3-center structure (Pd, S2, and C_{CH_3} atoms) with quasi-similar Pd–S distance (Pd–S2: 2.455 Å), a shorter Me–S₂ bond (2.316 Å) than the Me–S₃ one in $TS^{OA}1^B$, and a more slightly elongated C_{CH_3} –Pd bond (2.457 Å). Intrinsic reaction coordinate (IRC) calculations confirmed that these two TS are both connected to the same penta-coordinated intermediate ($1a^B$), where the methyl group is in apical position.

Case of the Labile Phosphine PPh_3 . To evaluate the influence of monodentate labile phosphines, we have explored the activation of S– CH_3 bond from the hypothetical $Pd^{II}(PPh_3)_2(\eta^1-L)_2$ complex, which involves slightly more

bulky phosphine groups (cone angle of 132° for PEt_3 and 145° for PPh_3).³² We turn our attention to predissociation mechanisms since the intermediate $Pd^{II}(PPh_3)(\eta^1-L)(\eta^2-L)$ has also been evidenced by NMR and X-rays. As previously noticed for $Pd^{II}(PEt_3)(\eta^1-L)(\eta^2-L)$, NBO analysis allowed us to identify a strong $n_{SMe} \rightarrow Pd$ interaction in the PPh_3 complex [Pd –S3: 2.417 Å, NBO analysis: $LP1(S3) \rightarrow Pd$: 9.2 kcal/mol and $LP2(S3) \rightarrow Pd$: 97.0 kcal/mol, Table S1]. This interaction, which is slightly more important than that with PEt_3 , as revealed by NBO analysis and the shortening of the Pd–S3 distance (theoretically and experimentally), is consistent with the electronic effect of the PPh_3 ligand (weaker σ -donor effect than PEt_3 which reduces charge on metal). The PPh_3 -predissociation step is even more kinetically and thermodynamically favored than that with PEt_3 phosphine [$\Delta G^\ddagger(TS^{disso}2^B)$: 8.9 kcal/mol and $\Delta G(trans-Pd^{II}(PPh_3)_2(\eta^1-L)_2 \rightarrow 2^B)$: –19.4 kcal/mol].³³ This highly exergonic step is in line with the nondetection of $[Pd^{II}(PPh_3)_2(\eta^1-L)_2]$ upon reaction of $Pd^{II}(PPh_3)_2Cl_2$ with CsL and the unique identification of complex $Pd^{II}(PPh_3)(\eta^1-L)(\eta^2-L)$ in the NMR spectrum at room temperature. Comparison of the energy profiles depicted in Figures 6 and 8 has shown that all the different intermediates (2^B and $2a^B$) and transition states are

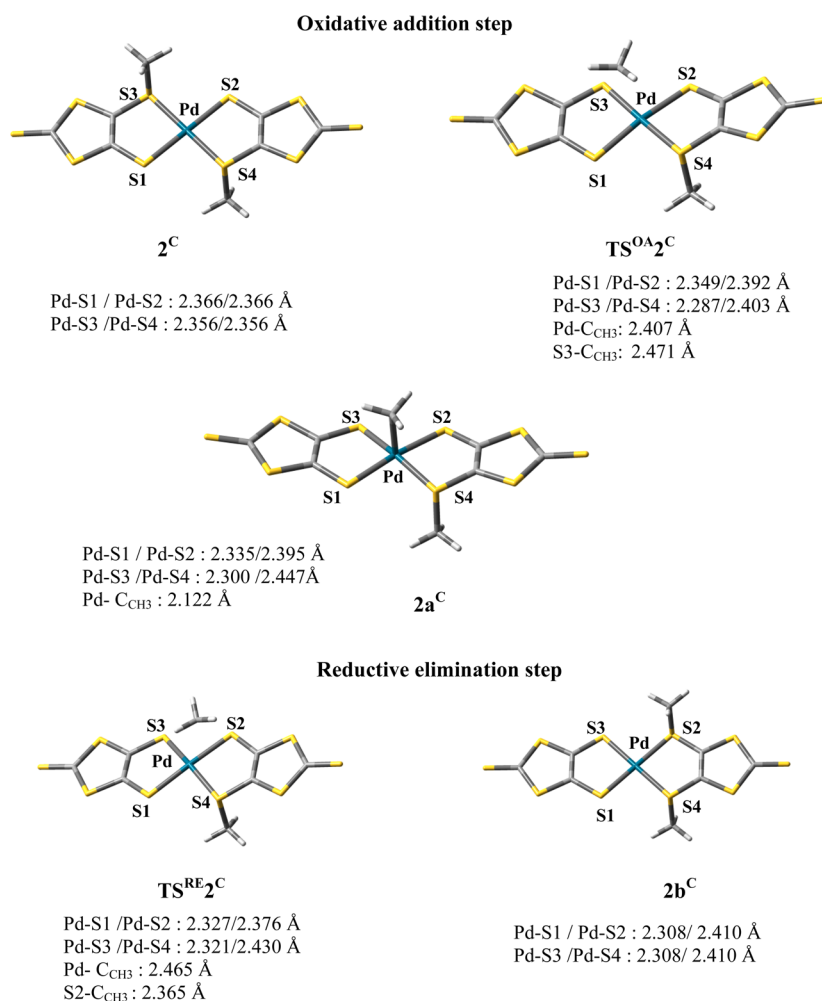
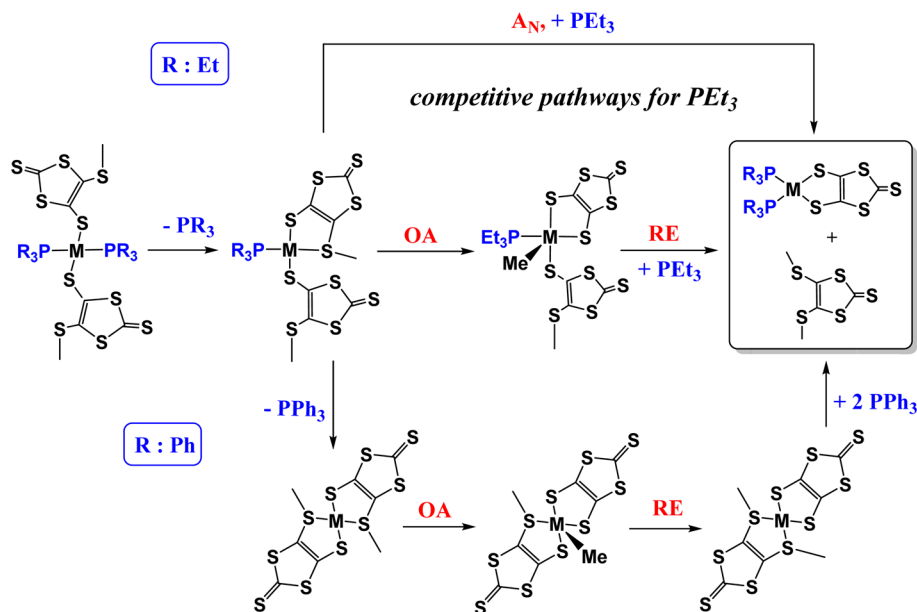
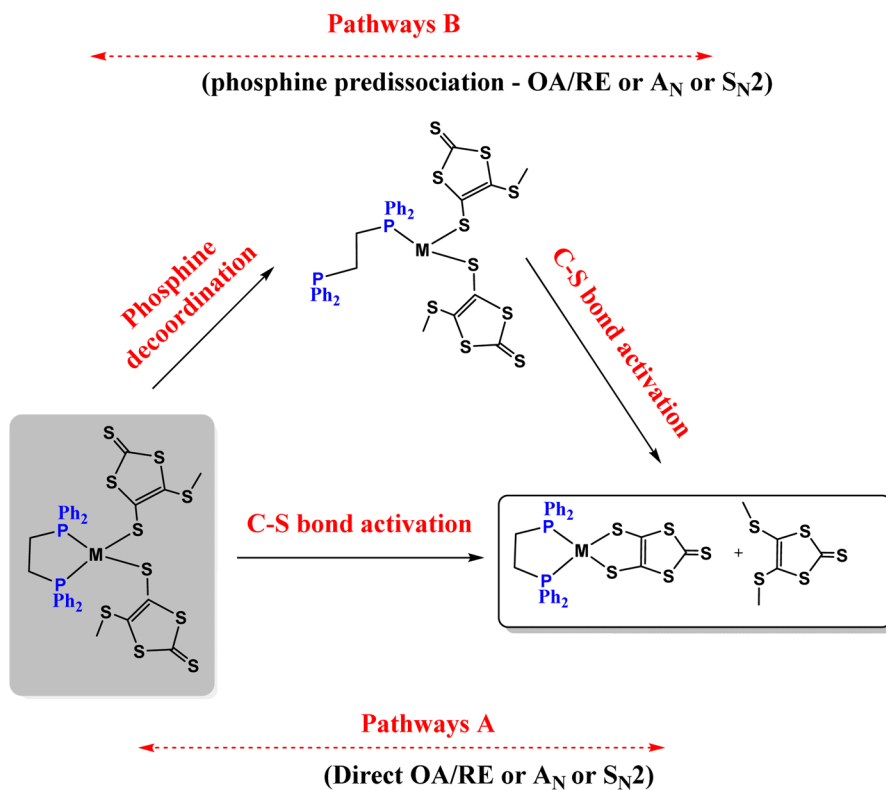


Figure 9. Main minima and TS involved in the oxidative addition/reductive elimination sequence for mechanism C, going through Pd^{II}(η²-L)₂ complex (2^C).

just downhill in energy by around 10 kcal/mol compared with those of the PEt₃ ligand. Thus, the activation barrier of the oxidative addition step is slightly decreased compared to that of the alkylphosphine ligand (~4 kcal/mol). The reductive elimination and nucleophilic substitution (B-A_N) steps are calculated to be similar to that with PEt₃, suggesting that the steric and electronic properties of the phosphine do not really affect this demethylation process. Likewise, the detailed examination of the optimized geometries of TS^{OA}2^B, TS^{RE}2^B, and TS^{AN}2^B evidences no noticeable difference with their PEt₃ analogues (see Figure S3). These preliminary results emphasize that a competition between oxidative addition/reductive elimination sequence (B-OA/RE) and nucleophilic addition (B-A_N) may also happen (difference around 0.5 kcal/mol between the two TS involved in RE and A_N reactions), as previously observed with PEt₃ ligand.

In light of the experimental data for Pd^{II}(PPh₃)(η¹-L)(η²-L) complex (dissociation of PPh₃ at high temperature and exchange between coordinated and free PPh₃), we have considered another pathway involving decooordination of the second phosphine group from Pd^{II}(PPh₃)(η¹-L)(η²-L) and going through Pd^{II}(η²-L)₂ intermediate (2^C, Scheme 6). The Pd^{II}(η²-L)₂ complex (2^C) has been found as minimum on the potential energy surface (PES). The dissociation of PPh₃ from Pd^{II}(PPh₃)(η¹-L)(η²-L) is straightforward under the exper-

imental conditions (363 K, Figure 3) and can afford easily Pd^{II}(η²-L)₂ complex (ΔG = -1.0 kcal/mol; ΔG[#]: 18.7 kcal/mol, Figure S4),³⁵ in line with the experimental NMR observations. The ability of demethylation from this intermediate (2^C) has been studied computationally (Figure 8) to compare with the mechanism (B-OA/RE) in Scheme 5. The activation barrier of the oxidative addition step was calculated relatively close with or without dissociation of the phosphine (ΔG[#] = 34.4 kcal/mol vs 34.1 kcal/mol from 2^C). In contrast, a higher difference was found for the reductive elimination step, where a decrease of the activation barrier around 7 kcal/mol was observed in the case of the mechanism involving Pd^{II}(η²-L).³⁶ Examination of the structures of the two TS for pathway C indicated (i) the concerted formation of Pd-C_{CH₃} bond (2.407 Å) and cleavage of S3-C_{CH₃} bond (2.471 Å) in TS^{OA}2^C as well as (ii) cleavage of Pd-C_{CH₃} bond (2.465 Å) and formation of S2-C_{CH₃} bond (2.365 Å) in TS^{RE}2^C. Comparison of the geometrical features of these transition states with those associated with pathway B-OA/RE revealed weak modifications in the oxidative addition step (See Figures S3 and 9, similar distances and ΣPd: 359.1° in TS^{OA}2^C versus ΣPd: 361.6° in TS^{OA}2^B), in agreement with similar activation barriers. In contrast, the changes are more important in the reductive elimination step. More specifically, the Pd center is more distorted in TS^{RE}2^B than in TS^{RE}2^C (ΣPd: 367.4° in

Scheme 7. Privileged Pathways for C–S Bond Activation from $M(PR_3)_2(\eta^1-L)_2$ Scheme 8. Plausible Mechanisms from C–S bond activation in $Pd^{II}(\eta^2-dppe)(\eta^1-L)_2$ complex^a

^aIncluding oxidative addition/reductive elimination sequence, nucleophilic substitution S_N2 , and nucleophilic addition. Pathways A correspond to direct pathways, and pathways B are those involving phosphine predissociation.

TS^{RE2^B} versus 359.6° for TS^{RE2^C}) because of steric constraint, which can be one of the reasons of the energy difference around 9 kcal/mol.

Intriguingly, the demethylation reaction was predicted to preferentially proceed through $Pd^{II}(\eta^2-L)_2$ intermediate (pathway C) rather than directly going through $Pd^{II}(PPh_3)(\eta^1-L)(\eta^2-L)$ complex (mechanisms B). This is pointed out by the energetic span δE , which has been calculated around 39.3 kcal/

mol for mechanism C versus for 47.6 for mechanism B-OA/RE and 47.1 for mechanism B- A_N .³⁷ As previously described for the OA/RE sequence in mechanism B with PEt_3 ligand, DFT calculations indicated that the oxidative step assumes an important role on the feasibility of the demethylation process. Indeed, penta-coordinated intermediate $2a^C$ (methyl group in apical position and the Pd atom surrounded by four sulfur atoms in a square planar environment) is not thermodynamically

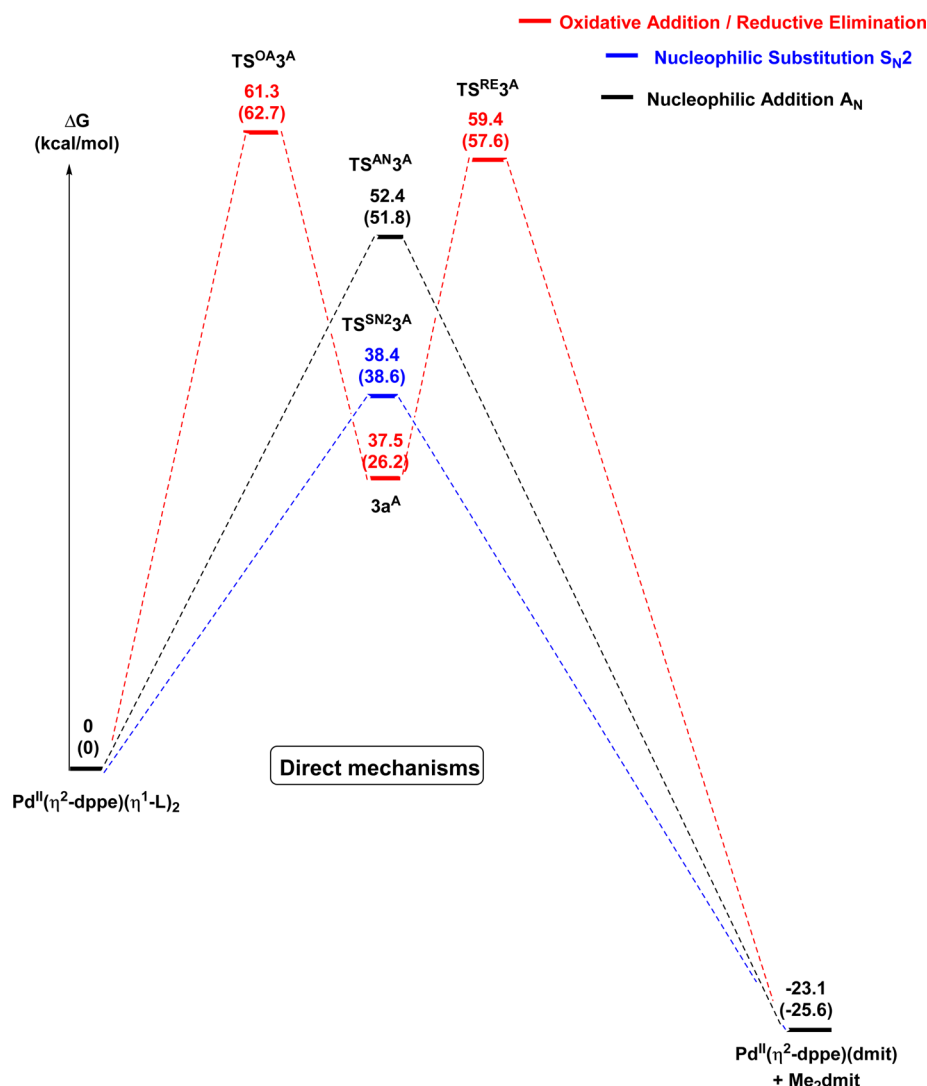


Figure 10. Energy profiles ($\Delta G^{\text{CH}_3\text{CN}}$ in kcal/mol) for the direct pathways (nucleophilic substitution $S_{\text{N}}2$, nucleophilic addition A_{N} , and oxidative addition/reductive elimination) for C–S bond activation from $\text{Pd}^{\text{II}}(\eta^2\text{-dppe})(\eta^1\text{-L})_2$ calculated at the B3LYP/SMD(CH_3CN)/SDD+f(M),6-31G** (other atoms)//B3LYP/SDD+f(M), 6-31G** (other atoms) level of theory. The values in parentheses are those obtained for the analogue Pt species.

cally favored. This results in a competition between two reductive elimination pathways. The first, corresponding to the reverse oxidative addition step, gives $\text{Pd}^{\text{II}}(\eta^2\text{-L})_2$, which can then be converted into $\text{Pd}^{\text{II}}(\text{PPh}_3)(\eta^1\text{-L})(\eta^2\text{-L})$ complex after phosphine coordination, and the second one leads to demethylation product $\text{Pd}^{\text{II}}(\text{PPh}_3)_2(\text{dmit})$. The weak thermodynamic preference for this dithiolene complex ($\Delta G \approx -4$ kcal/mol from 2^{C} or -5.1 kcal/mol from 2^{B}) and the readily accessible activation barrier to once again regenerate the kinetic product $\text{Pd}^{\text{II}}(\text{PPh}_3)(\eta^1\text{-L})(\eta^2\text{-L})$ from 2a^{C} perfectly agree with an inefficient demethylation reaction and are consistent with the experimental observations, i.e., a ratio of $\text{Pd}^{\text{II}}(\text{PPh}_3)(\eta^1\text{-L})(\eta^2\text{-L})/\text{Pd}^{\text{II}}(\text{PPh}_3)_2(\text{dmit})$ close to 20 upon heating the reactants $\text{Pd}(\text{PPh}_3)_2\text{Cl}_2$ and CsL at 348 K during 17 h.

Similarly, the high endergonicity of the oxidative addition step for the PEt_3 ligand tends to show that $\text{Pd}^{\text{II}}\text{PEt}_3(\eta^1\text{-L})(\eta^2\text{-L})$ species is the kinetically controlled product of the demethylation process ($\Delta G^\ddagger = 11.7$ kcal/mol for the reverse oxidative addition process versus $\Delta G^\ddagger = 22.8$ kcal/mol for the formation of $\text{Pd}^{\text{II}}(\text{PEt}_3)_2(\text{dmit})$ by RE from 1a^{B}). On the contrary, $\text{Pd}^{\text{II}}(\text{PEt}_3)_2(\text{dmit})$ seems to be the thermodynamically

controlled derivative and can originate from nucleophilic addition reaction from 1^{B} and/or reductive elimination from 1a^{B} . Finally, the improvement of the demethylation process with alkyl group on phosphorus (40/60 for PEt_3 versus 5/95 for PPh_3) can be correlated to higher thermodynamic stabilization of the dithiolene complex bearing a PEt_3 ligand compared to PPh_3 ($\Delta G^{\text{dithiolene}} = -9.9$ kcal/mol from 1^{B} versus $\Delta G^{\text{dithiolene}} = -4.7$ kcal/mol from 2^{B}).

Thus, all these results highlight that in heteroleptic monophosphine/L palladium complexes the C–S bond activation can occur via two competitive pathways: a nucleophilic addition reaction and/or an oxidative/reductive elimination sequence (Scheme 7). However, DFT calculations make a distinction between PEt_3 and PPh_3 derivatives. With PEt_3 , the two reactions take place simultaneously and directly from $\text{Pd}^{\text{II}}(\text{PEt}_3)(\eta^1\text{-L})(\eta^2\text{-L})$, whereas the dissociation of the triphenylphosphine from $\text{Pd}^{\text{II}}(\text{PPh}_3)(\eta^1\text{-L})(\eta^2\text{-L})$ implies that oxidative addition/reductive elimination mechanism is favored and occurs preferentially from $\text{Pd}^{\text{II}}(\eta^2\text{-L})_2$ complex. The thermodynamic stabilization of the final products [$\text{Pd}^{\text{II}}(\text{PR}_3)_2(\text{dmit}) + \text{Me}_2\text{dmit}$] compared to intermediate

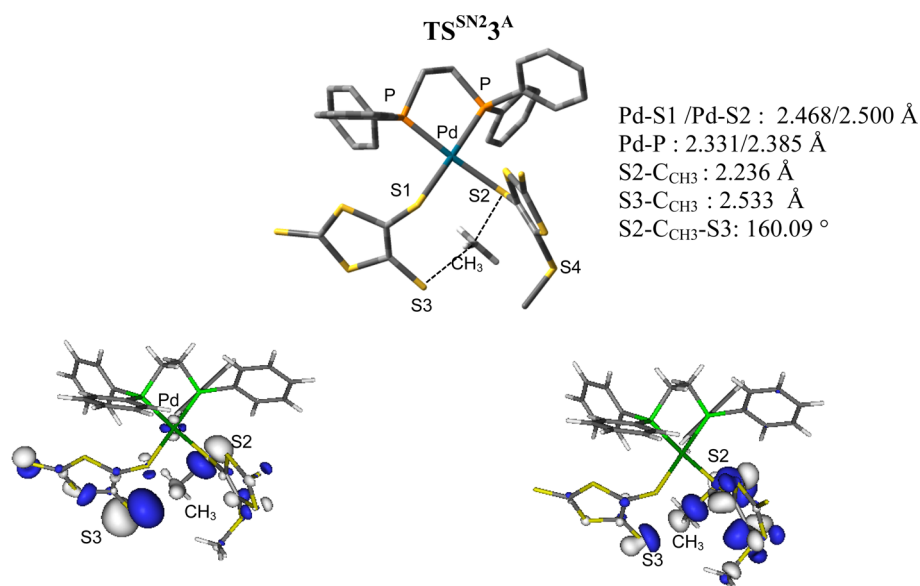


Figure 11. Main geometrical parameters of TS^{SN2}3^A (distances in Å and bond angles in deg) and main molecular orbitals (cutoff: 0.04) involved in direct S_N2 mechanism from Pd^{II}(η²-dppe)(η¹-L)₂.

Pd^{II}(PR₃)(η¹-L)(η²-L) seems to be the driving force for the efficiency of the process and suggests that the latter is under thermodynamic control (better yield with PEt₃). However, the relatively high activation barriers of RE and A_N steps are responsible for the poor yield of demethylation (<50%).

Case of the Chelate Phosphine dppe. To extend this work, the demethylation process has also been investigated with the strongly chelating diphosphine dppe, for which a pathway implying a predissociation of a phosphine arm appears *a priori* quite unlikely especially in the case of dppe. Nevertheless, the opening of a dppe chelate ring has been already proposed in mechanisms involving dihydrogen complex *trans*-[FeH(H₂)-(dppe)₂]⁺.³⁸ Therefore, we have theoretically considered both direct (pathways A) and indirect pathways (pathways B) from [Pd(η²-dppe)(η¹-L)₂] (Scheme 8).

The substitution of one phosphine arm by the thiomethyl group requires a slightly less accessible barrier than that for the monodentate phosphines (Figure S2) [ΔG^\ddagger (TS^{disso}3^B) = 19.7 kcal/mol versus 9–15 kcal/mol]. As expected, greater difference appears in the thermodynamic feasibility of this phosphine/thiomethyl exchange. While it was exergonic for the labile phosphines [PET: ΔG (TS^{disso}1^B) = -10.5 kcal/mol; PPh₃: ΔG (TS^{disso}2^B) = -19.4 kcal/mol], it is endergonic for the chelate dppe phosphine [ΔG (TS^{disso}3^B) = 8.3 kcal/mol], showing that the feasibility of this largely depends on the nature of the ligand and can be excluded with dppe.³⁹ Looking at the bonding situation in intermediate 3^B, no significant difference is observed (see Table S1) compared to those of the corresponding PEt₃ and PPh₃ analogues, indicating that the endergonicity of this step seems rather to be correlated to the higher stability of the chelate Pd^{II}(η²-dppe)(η¹-L)₂ complex. As might be expected, the oxidative addition step from 3^B is uphill by around 10–20 kcal/mol compared to those calculated for Pd^{II}(PR₃)₂(η¹-L)₂ complexes (ΔG^\ddagger (TS^{OA}3^B) = 44.7 kcal/mol, Figure S5), and the reductive elimination could not take place because the activation barrier is unreachable (ΔG^\ddagger (TS^{RE}3^B) = 53.5 kcal/mol). The nucleophilic addition (A_N) and substitution (S_N2) are also energetically disfavored (ΔG^\ddagger > 55

kcal/mol), ruling out any mechanisms involving dissociation of one phosphine arm (Figures S6 and S7).

Activation barriers for the direct oxidative addition/reductive elimination sequence and A_N pathway were also found very high in energy (Figure 10) [ΔG^\ddagger = 52–62 kcal/mol]. By contrast, the transition state lies around 38.4 kcal/mol over Pd^{II}(η²-dppe)(η¹-L)₂ for the intramolecular S_N2 mechanism. The barrier presents the same magnitude as that for the oxidative addition step in the predissociative pathway involving labile phosphines and can be therefore reached under the experimental conditions (~348 K in acetonitrile). It is noteworthy that S_N2 substitution at methyl group by chloride has also been proposed to account for the cleavage of Se–C(alkyl) bond in bis(alkyl)selenosalen Pd(II) and Pt(II) complexes (Scheme 1d),⁹ but in this latter example, the nucleophile (Cl⁻) is an external species.

The main geometric features of transition state TS^{SN2}3^A reveal simultaneous formation of a C_{CH3}...S₂^{thioether} bond (2.236 Å) and concomitant displacement of the Me group from S3 sulfur (2.533 Å), with a S2...Me...S3 bond angle being around 160.09°. Plots of the MOs involved in this reaction reinforces the intramolecular S_N2-like process (Figure 11), with HOMO–1 and LUMO+4 of TS corresponding to the S2 lone pair of the ligand L in interaction with the σ*_{S2C} orbital of the other ligand.

Examination of the geometric features of the initial reactants Pd^{II}(η²-dppe)(η¹-L)₂, *trans*-Pd^{II}(PEt₃)₂(η¹-L)₂, and their corresponding direct S_N2 transition states (TS^{SN2}3^A and TS^{SN2}1^A) reveals strong distortion of the geometry of the TS with PEt₃. In TS^{SN2}1^A, the metal presents a distorted square planar geometry compared to *trans*-Pd^{II}(PEt₃)₂(η¹-L)₂ (ΣPd: 374.1° versus ΣPd: 360.4°, see Figure S7) with a strong decrease of the S1PdS2 bond angle around 30–40° (173.6° in initial reactant and 137.21° in TS) and a decrease of P1MP2 around 13° (172.6° in initial reactant and 159.7° in TS). On the contrary, with dppe ligand, these main geometrical parameters remain quasi-similar in the two species (initial reactant ΣPd: 359.9°, S1MS2: 94.4°, and P1MP2: 86.6° versus TS, ΣPd: 360.0°, S1MS2: 92.1°, and P1MP2: 86.4°). These data confirm that the large difference between the direct S_N2 activation barriers of the

two systems originates from the bent PPdP (chelate phosphine) versus linear (*trans*-PEt₃ phosphines) geometry, pointing out that the chelate effect preorganizes the system for the S_N2 pathway, becoming thus the most favorable. This is confirmed by the localization of the S_N2 transition states from *cis*-Pd^{II}(PR₃)₂(η¹-L)₂ complexes (R = Et and Ph; see Figures S10 and S11 for the energy profiles and Figures S8 and S9 for the geometrical features), which present activation barriers (ΔG[‡] ≈ 30 kcal/mol) close to that computed from Pd^{II}(η²-dppe)(η¹-L), where no strong structural deformation was evidenced.

Influence of the Metal Center: Pd versus Pt. Finally, influence of the metal center (Pt versus Pd) was also examined, especially in the case of labile phosphines where the [M(PR₃)₂(*dmitt*)]/[M(PR₃)(η¹-L)(η²-L)] ratios have been experimentally determined. In line with the experimental observation, a lower lability of the phosphine ligand is computed in the case of the platinum complexes (Figure S2). The energy profiles of all the plausible mechanisms (Figures 6 and 8) were found to be very similar to those calculated for the palladium complexes, showing that the metal does not really impact the nature of the privileged pathway. The only noticeable differences between the two metal centers rest on two key points. The first one corresponds to the relative thermodynamic instability of oxidative addition product (**1a^B**/**2a^B** and **2a^C**), which makes this step more or less reversible and leads to reformation of M(PR₃)(η¹-L)(η²-L). Penta-coordinated intermediates **1a^B**/**2a^B** and **2a^C** appear to be more stable by around 8–10 kcal/mol with platinum than with palladium, consistent with a strengthening of the M–C bond.⁴⁰ Consequently, the oxidative addition step is facilitated with platinum center (lower reversibility), which can indirectly further privilege the formation of the demethylation product, as experimentally confirmed. The second point relates to the energy of the demethylation process from key intermediate [M(PR₃)(η¹-L)(η²-L)]. This C–S bond activation is more thermodynamically favored for the platinum complexes than for the palladium ones (ΔG_{rx} around –10 to –16 kcal/mol for Pt compared to –5 to –10 kcal/mol for Pd), indicating a better efficiency of the overall process for the platinum complexes (thermodynamic control).

CONCLUSION

In this contribution, we studied the coordination of mixed thiolate/thioether ligand **L** on Pd^{II}P₂ core and evidenced competition between formation of PdP₂(η¹-L)₂ and PdP(η¹-L)(η²-L) complexes depending on the nature of the phosphine. The S_{thioether}–Pd interaction substituted a P–Pd interaction with the monophosphines PEt₃ and PPh₃, whereas Pd(dppe)-(η¹-L)₂ was found to be stable at room temperature. With dppm, the coexistence in solution of both species Pd(η²-dppm)(η¹-L)₂ and Pd(η¹-dppm)(η¹-L)(η²-L) is observed. Experimental investigations revealed that the H₃C–S bond activation occurred at high temperature leading to heteroleptic phosphine/dithiolene complexes, PdP₂(*dmitt*) and MeL. In contrast to the other examples of C(sp³)–S bond cleavage reported in the literature, which are mainly described as resulting from substitution involving external nucleophile or are more scarcely photochemically induced, the thermal C–S bond activation reported in this work did not require the presence of an external reactant. Theoretical study by DFT calculations allowed us to establish the mechanism of the intramolecular C–S bond activation in these complexes. The latter depends on

the nature of the ancillary ligands. With the chelating dppe phosphine, an intramolecular S_N2 process in which a S_{thiolate} acts as nucleophile appears as most feasible pathway due to the cis position of η¹-L ligands imposed by the stable Pd(η²-dppe) metallacycle. With PPh₃ ligand, the C–S bond was found to be activated via an oxidative addition process leading to a penta-coordinated Pd^{IV} intermediate from the thermodynamically stable square planar Pd^{II}(η²-L) species, which after reductive elimination affords dithiolene complexes Pd^{II}(PPh₃)₂(*dmitt*). With the alkyl analogue (PEt₃), both nucleophilic addition A_N and oxidative addition/reductive elimination sequence may simultaneously occur through Pd^{II}(PEt₃)(η¹-L)(η²-L) complex, leading to the demethylation product. This C–S bond activation is under thermodynamic control, with the efficiency correlated with the thermodynamic stabilization of the demethylation product compared with key intermediate Pd(PR₃)(η¹-L)(η²-L). Theoretical calculations also point out that the nature of the metal Pt versus Pd does not impact the privileged pathway. The greater efficiency of the demethylation reaction generally observed with platinum complexes may result from the greater stability of the Pt^{II}P₂(dithiolene) products versus their Pd^{II} analogues. It should be also emphasized that the coordination sphere of the Pd^{II}/Pt^{II} impacts not only the mechanism of the S–CH₃ bond activation but also the reactivity of **L**. The coupling of two **L** ligands by reaction with PdCl₂ or PtCl₂ points out the influence of the ancillary ligands in the reactivity of **L** coordinated on Pd^{II} or Pt^{II} center.

EXPERIMENTAL SECTION

General. All manipulations were performed using Schlenk techniques in an atmosphere of dry oxygen-free argon. Elemental C, H, and S analyses were performed on a Leco Elemental Analyzer CHN 900. The ³¹P{¹H} NMR spectra were recorded at 121.50 MHz on a Bruker DRX 300 spectrometer. CsL,¹⁵ Pd(PPh₃)₂Cl₂,⁴¹ Pd(PEt₃)₂Cl₂,⁴² Pd(dppm)Cl₂,⁴³ and Pd(dppe)L₂ (**3**)¹³ (³¹P{¹H} NMR-CDCl₃: δ 59.6 ppm) were prepared according to the literature. Samples of Pd(η²-dppe)(*dmitt*), Pd(η²-dppm)(*dmitt*), Pd(PPh₃)₂(*dmitt*), and Pd(PEt₃)₂(*dmitt*) were prepared by reaction of the C₃S₅²⁻ ligand (*dmitt*) with the appropriate [PdCl₂P₂] precursor⁴⁴ and their ³¹P{¹H} NMR spectra were recorded (a singlet was observed at 56.7, –39.0, 26.9, and 18.5 ppm, respectively). The bulk purity of new compounds was established by NMR spectroscopy (¹H, ¹³C, and ³¹P) and elemental analyses.

Synthesis of Pd(PEt₃)(η¹-L)(η²-L) (1**).** To a methanol (25 mL) solution of *cis*-Pd(PEt₃)₂Cl₂ (0.041 g, 0.1 mmol) was added cesium 1,3-dithiole-2-thioxo-4-methylthio-5-thiolate (0.076 g, 0.22 mmol). The solution was refluxed for 5 h. After cooling to room temperature, the reaction mixture was filtered and the dark brown precipitate was extracted into dichloromethane. The extract was concentrated in vacuo to afford **1** (0.037 g, 57%). Single crystals of complex **1** were grown by keeping a solution of **1** in chloroform/hexane mixture for 2 days at 4 °C. Anal. Calcd for C₁₄H₂₁PPdS₁₀ (*M* = 647.4) C, 25.97 H, 3.27 S, 49.53; found: C, 26.17 H, 3.39 S, 49.23. ¹H NMR (295 K, CDCl₃, δ) 2.66 (s, 6H, CH₃), 2.02 (m, 6H, P–CH₂–), 1.23 (m, 9H, CH₂–CH₃) ppm. ¹³C{¹H} NMR (CDCl₃, δ) 8.3 (²J_{C–P} = 2.9 Hz), 15.9 (¹J_{C–P} = 31.1 Hz), 22.9(–CH₃), 121.9 (C4), 152.2 (C5, ³J_{C–P} = 4.4 Hz), 214.6 (C=S). ³¹P NMR (295 K, CDCl₃, δ) 35.7 ppm. IR (KBr disk, cm^{–1}): 1058 (ν_{C=S}), 743, 628, 511 (ν_{PEt3}). UV/vis (CH₂Cl₂, λ_{max} nm (ε, M^{–1} cm^{–1}): 306 (32857), 414 (20952).

Pd(PPh₃)(η¹-L)(η²-L) (2**).** Complex **2** was prepared by using precursor Pd(PPh₃)₂Cl₂ following the same procedure as that for complex **1** (70% yield). Anal. Calcd for C₂₆H₂₁PPdS₁₀ (*M* = 791.5) calcd C, 39.46 H, 2.67 S, 40.51; found: C, 39.68 H, 2.67 S, 40.17. ¹H NMR (295 K, CDCl₃, δ) 7.69–7.48 (m, 15 H, Ph), 2.61 (s, 6 H, CH₃) ppm. ¹³C{¹H} NMR (CDCl₃, δ) 23.0 (–CH₃), 121.5 (C4), 127.7

($^1J_{C-P} = 54.0$ Hz), 128.6 ($^2J_{C-P} = 11.2$ Hz), 131.8, 134.4 ($^3J_{C-P} = 10.9$ Hz), 153.1 (C=S), 214.6 (C=S). ^{31}P NMR (295 K, $CDCl_3$, δ) 32.6 ppm. IR (KBr disk, cm^{-1}): 1057 ($\nu_{C=S}$), 741, 692, 517 (ν_{PPh_3}). UV/vis (CH_2Cl_2) λ_{max} nm (ϵ , $M^{-1} cm^{-1}$): 311 (39762), 415 (21714).

Synthesis of Pd(dppm) $_2$ (4). Pd(dppm) $_2Cl_2$ (0.056 g, 0.1 mmol) and cesium 1,3-dithiole-2-thioxo-4-methylthio-5-thiolate (0.069 g, 0.2 mmol) were stirred in acetone (10 mL) at room temperature for 6 h. After evaporation of the solvent, the orange residue was extracted with CH_2Cl_2 (2×7 mL). Evaporation under reduced pressure afforded **3** as a red solid (0.068 g, 75%). Anal. Calcd for $C_{33}H_{28}P_2PdS_{10}$ ($M = 913.6$) calcd C, 43.38 H, 3.09 S, 35.10; found: C, 43.62 H, 3.17 S, 34.78. 1H NMR (295 K, $CDCl_3$, δ) 7.66–7.45 (m, 20 H, Ph), 4.15 (br s, 2 H, PCH $_2$ P), 2.58 (s, CH_3 (η^1-L)), 2.40 (s, CH_3 (η^1-L)(η^2-L)) ppm. ^{31}P NMR (295 K, $CDCl_3$, δ) –38.3 ([Pd(η^2 -dppm)(η^1-L) $_2$]), 27.5 (–Ph $_2$ P–Pd in [Pd(η^1 -dppm)(η^1-L)(η^2-L)], –23.25 (Ph $_2$ P–CH $_2$ in [Pd(η^1 -dppm)(η^1-L)(η^2-L)] ppm. IR (KBr disk, cm^{-1}): 1061 ($\nu_{C=S}$). UV/vis (CH_2Cl_2) λ_{max} nm: 308, 412. Note that due to an equilibrium between Pd(η^2 -dppm)(η^1-L) $_2$ and the coordination isomer Pd(η^1 -dppm)(η^1-L)(η^2-L) identification of all C signals was not possible in the $^{13}C\{^1H\}$ NMR (see Supporting Information).

Synthesis of L–L. Method A. To a solution of CsL (34 mg, 0.1 mmol) in ethanol (15 mL) was added 0.5 equiv of MCl_2 ($M = Pd$ or Pt) under inert atmosphere. The resulting suspension was refluxed for 5 h. Then, the mixture was cooled at room temperature and was filtered off. The dark residue was further dissolved in dichloromethane to obtain a clear yellow solution of the disulfide compound. Evaporation of the solvent afforded an orange colored powder which was recrystallized in dichloromethane-hexane mixture to get single crystals for X-ray diffraction (4.6 mg, 22% with $M = Pd$).

Method B. A batch of CsL (0.34 g, 1.0 mmol) was dissolved in 15 mL of distilled water to obtain a red solution in a Schlenk tube. Then, 0.01 mmol of sodium iodide (1.5 mg, 1 mol %) and 1.0 mmol of 30% H_2O_2 (0.11 mL) were added directly, and the mixture was stirred at room temperature for 24 h. Next day, a saturated aqueous solution (20 mL) of $Na_2S_2O_3$ was added to get an orange precipitate of the disulfide compound. The mixture was filtered off and washed thoroughly with water and cold methanol. The precipitate was dried under vacuum (0.085 g, 40%). Anal. Calcd for $C_8H_6S_{10}$ ($M = 422.7$) calcd C, 22.73 H, 1.43 S, 75.85; found: C, 22.85 H, 1.47 S, 75.48. 1H NMR ($CDCl_3$, 300 MHz, δ) 2.55 (s) ppm. $^{13}C\{^1H\}$ NMR ($CDCl_3$): 19.3 (–CH $_3$), 128.8, 147.6, 209.8 (C=S) ppm. IR (KBr disk, cm^{-1}): 1061 ($\nu_{C=S}$). UV/vis (CH_2Cl_2) λ_{max} nm (ϵ , $M^{-1} cm^{-1}$): 275 (13786), 384 (15714). Mp: 123 °C.

Crystal Structure Determinations. The crystal structure determinations were effected at 173.15(2) K on a Xcalibur, Sapphire3 diffractometer. The crystal was kept at 173.15 K during data collection. Using Olex2⁴⁵ the structure was solved with the ShelXT⁴⁶ structure solution program using Direct Methods and refined with the XL⁴⁷ refinement package using Least Squares minimization. Crystallographic parameters are listed in Table S2. CCDC-1489553 (**1**), 1489549 (**2**), and 1489552 (L–L) contain the supplementary crystallographic data for this paper. These data can be obtained free of charge from the Cambridge Crystallographic Data Centre via www.ccdc.cam.ac.uk/data_request/cif.

Computational Details. All calculations were performed using the Gaussian 09 package⁴⁸ and the B3LYP hybrid functional. B3LYP⁴⁹ is a three-parameter functional developed by Becke which combines the Becke gradient-corrected exchange functional and the Lee–Yang–Parr and Vosko–Wilk–Nusair correlation functionals with part of exact HF exchange energy. Palladium and platinum atoms were described with the relativistic electron core potential SDD and associated basis set,⁵⁰ augmented by a set of f-orbital polarization functions⁵¹ and 6-31G** basis set were employed for other atoms.

Optimization of the different minima and TS were carried out without any symmetry restrictions in gas phase. All total energies and Gibbs free energies have been zero-point energy (ZPE) and temperature corrected using unscaled density functional frequencies. Frequency calculations were undertaken to confirm the nature of the stationary points, yielding one imaginary frequency for transition states, corresponding to the expected process, and zero for minima.

The connectivity of the transition states and their adjacent minima was confirmed by intrinsic reaction coordinate (IRC) calculations.⁵² In addition, single-point calculations were carried out on the geometries obtained in gas phase, including the solvent (acetonitrile, CH_3CN) by means of the SMD implicit solvation model.⁵³ The electronic energies were then ZPE and temperature corrected based on full gas-phase-optimized geometry in order to obtain ΔH^{CH_3CN} and ΔG^{CH_3CN} values. Natural bond orbital⁵⁴ analyses (NBO, 5.9 version)⁵⁵ have been used to describe the bonding situation in the intermediates **1^B**, **2^B**, and **3^B**. Molecular orbitals were plotted with Molekel 5.4.⁵⁶ The energetic span (δE) has been calculated in the case of the reactivity of *trans*-Pd^{II}(PPh $_3$) $_2$ (η^1-L) $_2$ in order to discriminate between mechanisms C and B-OA/RE. It corresponds to the energetic difference between TOF-determining intermediate (TDI) [Pd^{II}(PPh $_3$)(η^1-L)(η^2-L) for mechanism B-OA/RE and Pd^{II}(η^2-L) $_2$ for mechanism C] and the TOF-determining transition state (TDTS, reductive elimination TS).²⁹

■ ASSOCIATED CONTENT

Supporting Information

The Supporting Information is available free of charge on the ACS Publications website at DOI: 10.1021/acs.organomet.7b00039.

Cartesian coordinates (XYZ)

Crystallographic information for **1**, **2**, and L–L (CIF)

UV–visible spectrum of **2**, energy profiles for $MP_2(\eta^1-L)_2$ complexes, NBO analysis of the intermediate **1^B**, **2^B** and **3^B**, main minima and TS, energy profiles, free energy profiles, energy for the phosphine-predissociation pathway, main bond angles in the initial reactants and corresponding TS, NMR spectra of **1**, **2**, **4** and L–L (PDF)

■ AUTHOR INFORMATION

Corresponding Authors

*E-mail: fabrice.guyon@univ-fcomte.fr.

*E-mail: karinne.miqueu@univ-pau.fr.

ORCID

Fabrice Guyon: 0000-0001-8905-2904

Notes

The authors declare no competing financial interest.

■ ACKNOWLEDGMENTS

Financial support from the Centre National de la Recherche Scientifique, the Université de Franche-Comté (post-doctoral grant to S.K.) and Université de Pau et des Pays de l'Adour (UPPA) are gratefully acknowledged. UPPA, MCIA (Mésocentre de Calcul Intensif Aquitain), and IDRIS under Allocation 2016 (i2016080045) made by Grand Equipement National de Calcul Intensif (GENCI) are also acknowledged for computational facilities.

■ REFERENCES

- Blomstrand, C. W. *J. Prakt. Chem.* **1883**, 27, 161–198.
- (a) Pan, F.; Shi, Z.-J. *ACS Catal.* **2014**, 4, 280–288. (b) Wang, L.; He, W.; Yu, Z. *Chem. Soc. Rev.* **2013**, 42, 599–621. (c) Modha, S. G.; Mehta, V. P.; Van der Eycken, E. *Chem. Soc. Rev.* **2013**, 42, 5042–5055. (d) Desnoyer, A. N.; Love, J. A. *Chem. Soc. Rev.* **2017**, 46, 197–238. (e) Ouch, K.; Mashuta, M. S.; Grapperhaus, C. A. *Inorg. Chem.* **2011**, 50, 9904–9914. (f) Sargent, A. L.; Titus, E. P. *Organometallics* **1998**, 17, 65–77. (g) Angelici, R. J. *Organometallics* **2001**, 20 (7), 1259–1275. (h) Kuniyasu, H.; Ohtaka, A.; Nakazono, T.; Kinomoto, M.; Kurosawa, H. *J. Am. Chem. Soc.* **2000**, 122, 2375–2376.

- (3) (a) Lindoy, L. F. *Coord. Chem. Rev.* **1969**, *4*, 41–71. (b) Lindoy, L. F.; Livingstone, S. B.; Lockyer, T. N. *Inorg. Chem.* **1967**, *6*, 652–656. (c) Lockyer, T. N. *Aust. J. Chem.* **1974**, *27*, 259–267. (d) Sacconi, L.; Speroni, G. P. *Inorg. Chem.* **1968**, *7*, 295–299. (e) Roundhill, D. M.; Beaulieu, W. B.; Bagchi, U. *J. Am. Chem. Soc.* **1979**, *101*, 5428–5430.
- (4) Kim, J. S.; Reibenspies, J. H.; Darensbourg, M. T. *J. Am. Chem. Soc.* **1996**, *118*, 4115–4123.
- (5) Schrauzer, G. N.; Rabinowitz, H. N. *J. Am. Chem. Soc.* **1968**, *90*, 4297–4302. (b) Ohkoshi, S.; Ohba, Y.; Iwaizumi, M.; Yamauchi, S.; Ohkoshi-Ohtani, M.; Tokuhisa, K.; Kajitani, M.; Akiyama, T.; Sugimori, A. *Inorg. Chem.* **1996**, *35*, 4569–4574.
- (6) (a) Benefiel, A.; Roundhill, D. M. *Inorg. Chem.* **1986**, *25*, 4027–4031. (b) Benefiel, A.; Roundhill, D. M.; Fultz, W. C.; Rheingold, A. L. *Inorg. Chem.* **1984**, *23*, 3316–3324.
- (7) Mandal, S.; Paul, N.; Banerjee, P.; Mondal, T. K.; Goswami, S. *Dalton Trans.* **2010**, *39*, 2717–2726.
- (8) (a) Takeda, N.; Tanaka, Y.; Oma, R.; Sakakibara, F.; Unno, M. *Bull. Chem. Soc. Jpn.* **2016**, *89*, 922–930. (b) Takeda, N.; Tanaka, Y.; Sakakibara, F.; Unno, M. *Bull. Chem. Soc. Jpn.* **2010**, *83*, 157–164.
- (9) (a) Panda, S.; Rama Krishna, G.; Reddy, C. M.; Zade, S. S. *Dalton Trans.* **2011**, *40*, 6684–6690. (b) Dutta, P. Kr.; Panda, S.; Rama Krishna, G.; Reddy, C. M.; Zade, S. S. *Dalton Trans.* **2013**, *42*, 476–483.
- (10) Kim, S.; Boyle, P. D.; McCreedy, M. S.; Pellarin, K. R.; Puddephatt, R. J. *Chem. Commun.* **2013**, *49*, 6421–6423.
- (11) Guyon, F.; Knorr, M.; Garillon, A.; Strohmman, C. *Eur. J. Inorg. Chem.* **2012**, *2012*, 282–291.
- (12) Sgro, M. J.; Stephan, D. W. *Organometallics* **2012**, *31*, 1584–1587.
- (13) (a) Svenstrup, N.; Becher, J. *Synthesis* **1995**, *1995*, 215–235. (b) Rauchfuss, T. B.; Stiefel, E. I. *Prog. Inorg. Chem.* **2003**, *52*, 1–54.
- (14) (a) Garreau-de Bonneval, B.; Moineau-Chane Ching, K. L.; Alary, F.; Bui, T.-T.; Valade, L. *Coord. Chem. Rev.* **2010**, *254*, 1457–1467. (b) Kosaka, Y.; Yamamoto, H. M.; Nakao, A.; Tamura, M.; Kato, R. *J. Am. Chem. Soc.* **2007**, *129*, 3054–3055. (c) Cassoux, P. *Coord. Chem. Rev.* **1999**, *185–186*, 213–232.
- (15) Zeltner, S.; Olk, R.-M.; Joerchel, P.; Sieler, J. Z. *Anorg. Allg. Chem.* **1999**, *625* (2), 368–373.
- (16) (a) Basolo, F.; Chatt, J.; Gray, H. B.; Pearson, R. G.; Shaw, B. L. *J. Chem. Soc.* **1961**, 2207–2215. (b) Wilkins, R. G. *Kinetics and Mechanism of Reactions of Transition Metal Complexes*; Wiley-VCH: New York, 2002.
- (17) (a) Miranda, S.; Cerrada, E.; Luquin, A.; Mendia, A.; Laguna, M. *Polyhedron* **2012**, *43*, 15–21. (b) Vinas, C.; Cirera, M. R.; Teixidor, F.; Sillanpaa, R.; Kivekas, R. *J. Organomet. Chem.* **1997**, *530*, 89–94.
- (18) Cordero, B.; Gomez, V.; Platero-Prats, A. E.; Reves, M.; Echeverria, J.; Cremades, E.; Barragan, F.; Alvarez, S. *Dalton Trans.* **2008**, 2832–2838.
- (19) Wrixon, J. D.; Hayward, J. J.; Rawson, J. M. *Inorg. Chem.* **2015**, *54*, 9384–9386.
- (20) Martinez, J.; Adrio, L. A.; Antelo, J. M.; Pereira, M. T.; Fernandez, J. J.; Vila, J. M. *Polyhedron* **2006**, *25*, 2848–2858.
- (21) (a) Chandrasekaran, P.; Greene, A. F.; Lillich, K.; Capone, S.; Mague, J. T.; DeBeer, S.; Donahue, J. P. *Inorg. Chem.* **2014**, *53*, 9192–9205. (b) Wrixon, J. D.; Ahmed, Z. S.; Anwar, M. U.; Beldjoudi, Y.; Hamidouche, N.; Hayward, J. J.; Rawson, J. *Polyhedron* **2016**, *108*, 115–121.
- (22) (a) Van Wart, H. E.; Lewis, A.; Scheraga, H. A.; Saeva, F. D. *Proc. Natl. Acad. Sci. U. S. A.* **1973**, *70*, 2619–2673. (b) David, C. Ph.D. Dissertation. Université de Franche-Comté, Besançon, France, 2009.
- (23) Breitzer, J. G.; Smirnov, A. I.; Szczepura, I. F.; Wilson, S. R.; Rauchfuss, T. B. *Inorg. Chem.* **2001**, *40*, 1421–1429.
- (24) Galloway, C. P.; Doxsee, D. D.; Fenske, D.; Rauchfuss, T. B.; Wilson, S. R.; Yang, X. *Inorg. Chem.* **1994**, *33*, 4537–4544.
- (25) Aida, M.; Nagata, C. *Theor. Chim. Acta* **1986**, *70*, 73–80.
- (26) (a) Shimizu, D.; Takeda, N.; Tokitoh, N. *Chem. Commun.* **2006**, 177–179. (b) Hunter, R.; Caira, M.; Stellenboom, N. *J. Org. Chem.* **2006**, *71*, 8268–8271. (c) Antoniow, S.; Witt, D. *Synthesis* **2007**, *2007*, 363–366. (d) Sanz, R.; Aguado, R.; Pedrosa, M. R.; Arnáiz, F. *Synthesis* **2002**, *2002*, 856–858. (e) Khazaei, A.; Zolfigol, M. A.; Rostami, A. *Synthesis* **2004**, 2959–2961. (f) Bao, M.; Shimizu, M. *Tetrahedron* **2003**, *59*, 9655–9659. (g) Uemura, S. In *Comprehensive Organic Synthesis*; Trosty, B. M., Fleming, I., Eds.; Pergamon Press: Oxford, 1991; Vol. 7, p 757. (h) Tam, J. P.; Wu, C.-R.; Liu, W.; Zhang, J.-W. *J. Am. Chem. Soc.* **1991**, *113*, 6657–6662.
- (27) Kirihara, M.; Asai, Y.; Ogawa, S.; Noguchi, T.; Hatano, A.; Hirai, Y. *Synthesis* **2007**, *2007* (21), 3286–3289.
- (28) Wrixon, J. D.; Hayward, J. J.; Raza, O.; Rawson, J. *Dalton Trans.* **2014**, *43*, 2134–2139.
- (29) The structural parameters of PtP₂S₂ complexes in which P-donor ligands are only organomonophosphines have been recently analyzed. With monodentate thiolates, 21 of the 31 examples exhibit a trans configuration: Melnik, M.; Mikus, P. *Rev. Inorg. Chem.* **2016**, *36*, 43–51.
- (30) Reoordination of the phosphine (**1b**^B + PEt₃ → M^{II}(PEt₃)₂dmit + Me₂dmit) requires a barrier around $\Delta G^\ddagger = 18.5$ kcal/mol ($\Delta H^\ddagger = 6.7$ kcal/mol) for Pd complex and $\Delta G^\ddagger = 30.9$ kcal/mol ($\Delta H^\ddagger = 18.5$ kcal/mol) for the Pt one.
- (31) Even if there is a possible overestimation by our calculations of the entropic effect, the formation of **1**^B remains favorable ($\Delta H = 2.3$ kcal/mol, Figure S2).
- (32) Tolman, C. A. *Chem. Rev.* **1977**, *77*, 313–348.
- (33) $\Delta H^{\text{CH}_3\text{CN}}$ values are also consistent with this experimental observation: $\Delta H^{\text{CH}_3\text{CN}}_{\text{PPh}_3} = -3.8$ kcal/mol < $\Delta H^{\text{CH}_3\text{CN}}_{\text{PEt}_3} = 2.3$ kcal/mol (Figure S2). Consequently, even if entropic effects are overestimated, they do not alter our conclusion (easier dissociation of the phosphine with PPh₃ ligand).
- (34) For the palladium complex, reoordination of the first phosphine (**2b**^C + PPh₃ → **2b**^B, $\Delta G^\ddagger = 22.3$ kcal/mol; $\Delta H^\ddagger = 9.5$ kcal/mol) requires an activation barrier similar to the second one (**2b**^B + PPh₃ → Pd^{II}(PPh₃)₂dmit + Me₂dmit, $\Delta G^\ddagger = 18.7$ kcal/mol; $\Delta H^\ddagger = 10.4$ kcal/mol).
- (35) The TS associated to the phosphine deoordination from Pd^{II}(PPh₃)($\eta^1\text{-L}$)($\eta^2\text{-L}$) is a late transition state with a Pd–P distance around 2.918 Å and a Pd–S(Me) of 2.477 Å quasi-formed (other Pd–S distances: 2.37–2.41 Å).
- (36) The TS corresponding to a A_N mechanism is high in energy ($\Delta G^\ddagger = 52.9$ kcal/mol) and is consequently unlikely.
- (37) (a) Kozuch, S. *WIREs Comput. Mol. Sci.* **2012**, *2*, 795–815. (b) Kozuch, S.; Shaik, S. *Acc. Chem. Res.* **2011**, *44*, 101–110. (c) Uhe, A.; Kozuch, S.; Shaik, S. *J. Comput. Chem.* **2011**, *32*, 978–985.
- (38) (a) Basallote, M. G.; Durán, J.; Fernández-Trujillo, M. J.; Manez, M. A. *J. Organomet. Chem.* **2000**, *609* (1–2), 29–35. (b) Basallote, M. G.; Durán, J.; Fernández-Trujillo, M. J.; González, G.; Máñez, M. A.; Martínez, M. *Inorg. Chem.* **1998**, *37*, 1623–1628.
- (39) The same conclusion can be drawn on the basis of the $\Delta H^{\text{CH}_3\text{CN}}$ values: $\Delta H^{\text{CH}_3\text{CN}}_{\text{dppe}} = 12.0$ kcal/mol > $\Delta H^{\text{CH}_3\text{CN}}_{\text{PEt}_3} = 2.3$ kcal/mol > $\Delta E^{\text{CH}_3\text{CN}}_{\text{PPh}_3} = -3.8$ kcal/mol (Figure S2).
- (40) (a) Luo, Y. R. *Comprehensive Handbook of Chemical Bond Energies*; CRC Press, Boca Raton, FL, 2007. (b) Citir, M.; Metz, R. B.; Belau, L.; Ahmed, M. *J. Phys. Chem. A* **2008**, *112*, 9584–9590. (c) Skinner, H. A.; Connor, J. A. *Pure Appl. Chem.* **1985**, *57*, 5779–5788.
- (41) Miyaura, N.; Suzuki, A. *Org. Synth.* **1990**, *68*, 130–136.
- (42) Doyle, J. R.; Slade, P. E.; Jonassen, H. B.; Rhoda, R. N. *Inorg. Synth.* **1960**, *6*, 216–219. (b) Hartley, F. R. *Organomet. Chem. Rev. A* **1970**, *6*, 119–137.
- (43) Steffen, W. L.; Palenik, G. J. *Inorg. Chem.* **1976**, *15*, 2432–2439.
- (44) Vicente, R.; Ribas, J.; Cassoux, P. *Nouv. J. Chim.* **1984**, *8*, 653–658.
- (45) Dolomanov, O. V.; Bourhis, L. J.; Gildea, R. J.; Howard, J. A. K.; Puschmann, H. *J. Appl. Crystallogr.* **2009**, *42*, 339–341.
- (46) Sheldrick, G. M. *Acta Crystallogr., Sect. A: Found. Adv.* **2015**, *71*, 3–8.

(47) Sheldrick, G. M. *Acta Crystallogr., Sect. A: Found. Crystallogr.* **2008**, *64*, 112–122.

(48) Frisch, M. J.; Trucks, G. W.; Schlegel, H. B.; Scuseria, G. E.; Robb, M. A.; Cheeseman, J. R.; Scalmani, G.; Barone, V.; Mennucci, B.; Petersson, G. A.; Nakatsuji, H.; Caricato, M.; Li, X.; Hratchian, H. P.; Izmaylov, A. F.; Bloino, J.; Zheng, G.; Sonnenberg, J. L.; Hada, M.; Ehara, M.; Toyota, K.; Fukuda, R.; Hasegawa, J.; Ishida, M.; Nakajima, T.; Honda, Y.; Kitao, O.; Nakai, H.; Vreven, T.; Montgomery, J. A., Jr.; Peralta, J. E.; Ogliaro, F.; Bearpark, M.; Heyd, J. J.; Brothers, E.; Kudin, K. N.; Staroverov, V. N.; Kobayashi, R.; Normand, J.; Raghavachari, K.; Rendell, A.; Burant, J. C.; Iyengar, S. S.; Tomasi, J.; Cossi, M.; Rega, N.; Millam, J. M.; Klene, M.; Knox, J. E.; Cross, J. B.; Bakken, V.; Adamo, C.; Jaramillo, J.; Gomperts, R.; Stratmann, R. E.; Yazyev, O.; Austin, A. J.; Cammi, R.; Pomelli, C.; Ochterski, J. W.; Martin, R. L.; Morokuma, K.; Zakrzewski, V. G.; Voth, G. A.; Salvador, P.; Dannenberg, J. J.; Dapprich, S.; Daniels, A. D.; Farkas, O.; Foresman, J. B.; Ortiz, J. V.; Cioslowski, J.; Fox, D. J. *Gaussian 09*, revision C.01; Gaussian, Inc.: Wallingford, CT, 2009.

(49) (a) Becke, A. D. *J. Chem. Phys.* **1993**, *98*, 5648–5652. (b) Becke, A. D. *Phys. Rev. A: At, Mol, Opt. Phys.* **1988**, *38*, 3098–3100. (c) Lee, C.; Yang, W.; Parr, R. G. *Phys. Rev. B: Condens. Matter Mater. Phys.* **1988**, *37*, 785–789.

(50) Andrae, D.; Häussermann, U.; Dolg, M.; Stoll, H.; Preub, H. *Theor. Chim. Acta* **1990**, *77*, 123–141.

(51) Ehlers, A. W.; Böhme, M.; Dapprich, S.; Gobbi, A.; Höllwarth, A.; Jonas, V.; Köhler, K. F.; Stegmann, R.; Veldkamp, A.; Frenking, G. *Chem. Phys. Lett.* **1993**, *208*, 111–114.

(52) (a) Gonzalez, C.; Schlegel, H. B. *J. Chem. Phys.* **1989**, *90*, 2154–2161. (b) Gonzalez, C.; Schlegel, H. B. *J. Phys. Chem.* **1990**, *94*, 5523–5527.

(53) Marenich, A. V.; Cramer, C. J.; Truhlar, D. G. *J. Phys. Chem. B* **2009**, *113*, 6378–6396.

(54) (a) Reed, E.; Curtiss, L. A.; Weinhold, F. *Chem. Rev.* **1988**, *88*, 899–926. (b) Foster, J. P.; Weinhold, F. *J. Am. Chem. Soc.* **1980**, *102*, 7211–7218. (c) Reed, A. E.; Weinhold, F. *J. Chem. Phys.* **1985**, *83*, 1736–1740.

(55) Glendening, E. D.; Badenhoop, J. K.; Reed, A. E.; Carpenter, J. E.; Bohmann, J. A.; Morales, C. M.; Weinhold, F. *NBO 5.0*; Theoretical Chemistry Institute, University of Wisconsin: Madison, 2001.

(56) Varetto, U. *MOLEKEL 5.4*; Swiss National Supercomputing Centre: Lugano, Switzerland, 2012.